A Quantitative Comparison of the Material-Use for a Form Found and a Conventional Concrete Pedestrian Bridge

By

A. Kariouh

Additional thesis
Delft University of Technology,

Supervisors:
Dr. M. Popescu, TU Delft
N. Christidi, MSc, TU Delft

2022

Contents

Abstract

Concrete is the most used building material in the world. Its success can be linked back to its mouldability, durability and low cost. Unfortunately, current conventional concrete pedestrian bridge designs do not benefit from these key features and still require bulky shaped cross-sections, whereby part of the concrete does not contribute to the structural strength. This study assesses the potential reduction of material use by combining shotcrete 3D printing (SC3DP) with the application of textile formworks for the production of form found pedestrian bridges, instead of the conventional design and fabrication process.

The present thesis looks at conventional concrete pedestrian bridge design and form found concrete for it examined for four different spans: 5 m, 10 m, 20 m and 45 m. The designs are tested for full vertical loading, asymmetric vertical loading, and buckling. The amount of material required for each span and load case are determined and compared with each other. The results show that the form found concrete pedestrian bridge designs only require a fraction (between 13.0% and 20.0%) of the amount of concrete used for the same design with conventional approaches. The form found concrete pedestrian bridge designs become more material efficient than the conventional designs as the span increases. During the calculation process it was ascertained that the conventional concrete pedestrian bridge design cannot reach spans larger than 20 m. It was also observed that the concrete thickness of the shorter span form found concrete pedestrian bridges (5 m and 10 m) is governed by the asymmetric load case and the concrete thickness of the longer span form found concrete pedestrian bridges (20 m and 45 m) is governed by the buckling case. Overall it can be concluded that the form found concrete pedestrian bridge design is superior with regards to the material use, when compared to the conventional concrete pedestrian bridge design.

Chapter 1

Introduction

1.1 Background

1.1.1 Architectural geometry

Majority of the conventional concrete bridge designs are based on rules of thumb that are founded on years of experience. These bridges are designed to carry their loads using bending action. Whereby the compression stresses at the top part of the deck are carried by the concrete and the tensile stresses, at the bottom of the deck are carried by the steel reinforcement. The bending moment resistance depends on the internal lever arm length (i.e. the depth of the structure). This results in very bulky cross-sections, whereby part of the concrete does not have a structural function and only is used to connect the reinforcement with the concrete at the top of the cross-section.

Form-found geometries are the result of structural optimization, with the objective to minimize the amount of material used (Adriaenssens et al., 2014). Physical form finding has been used by many architects and structural engineers in the 20th century to create lightweight structures (Veenendaal & Block, 2012). Currently computational form finding is used to determine the geometry of these structures.

Structures that contain less material must rely on geometry and rigorous placement of material where it is needed, such as the natural flow of forces, to obtain their stiffness. Bridges such as the one designed by Striatus by Zaha Hadid Architect and ETH Zürich (Figure 1.1a), the Töss footbridge by Robert Maillart (Figure 1.1b), and the Dyckerhoff Bridge by Gerd Lohmer (Figure 1.1c) are all examples how form finding can result in elegant and material efficient structure.

(a)

(b)

(c)

Figure 1.1: (a) Striatus 3D Printed Concrete Bridge by Zaha Hadid Architects and ETH Zürich, Venice, Italy, 2021; (b) Töss footbridge by Robert Maillart, Winterthur, Switzerland, 1933; (c) Dyckerhoff Bridge by Gerd Lohmer, Wiesbaden, Germany, 1967. (photo credit: (a) Naaro; (b) Nicolas Janberg; (c) Martin).

1.1.2 Problem statement

Concrete is the most widely used construction material. The annual worldwide production of concrete is estimated to be approximately 10 Gt (Meyer, 2004). This quantity of consumption causes cement (the strength-inducing binding component of concrete) manufacturing alone to account for 5-8% of the world's anthropogenic carbon emission (Castaldelli et al., 2014). With the existing stress on the environment, more efficient and sustainable use of concrete is needed.

Fresh concrete has the ability to be moulded in any preferred shape. This allows architects and structural engineers to economically create concrete structures with complex geometries. Unfortunately, this unique fluidity is seldom exploited, instead concrete is cast in rigid, rectangular formworks to create non-optimized geometries that give rise to cumbersome structures with a high material-use and large carbon footprints.

For the cases in which this fluidity of concrete is capitalized upon, the fabrication process still requires large custom-made formworks that cannot be reused and are discarded after a single use. According to García de Soto et al., (2018) these formworks account for 73% of the costs of a custom shaped structures.

1.1.3 Vision

Flexible formworks already have proven to work for the construction of lightweight concrete structures. Examples of such structures are the Concrete Shell Bridge by Block Research Group, ETH Zürich (Figure 1.2a), which uses the KnitCrete technology, and the NEST HiLo roof prototype by Block Research Group, ETH Zürich (Figure 1.2b), which is built using a woven fabric formwork. Alternatively, additive manufacturing has proven throughout the years to be capable of producing optimized structures with material

placement specificly at the locations where necessary. Different types of additive manufacturing of concrete have been developed, like extruded 3D concrete printing (E3DCP) and shotcrete 3D printing (SC3DP). Yet, there has not been a study that combined concrete 3D printing with knitted formworks to specifically deposit concrete at the required location and with the needed thickness.

(a) (b)

Figure 1.2: (a) The Concrete Shell Bridge by Block Research Group, ETH Zürich, 2018, NEST HiLo roof prototype by Block Research Group, ETH Zürich, 2019. (photo credit: (a) BRG; (b) Juney Lee).

1.2 Research objective

The main objective of this research is to:

Assess the potential reduction of material use by combining shotcrete 3D printing (SC3DP) with the application of textile formworks for the production of form found pedestrian bridges, instead of the conventional design and fabrication process.

The assessment consists of a quantitative comparison. Hereby, the amount of material used for the construction of a solid slab pedestrian bridge design is compared with the amount of material used for a form found pedestrian bridge design, for multiple spans. The method used for this assessment consists of the following three pillars:

- **Design:** defining the geometry of the bridges, the thickness of the concrete, the type of concrete used, and the dimensions of the steel reinforcement (in case used).
- **Calculation:** determining the magnitude of the governing internal forces and moments at the ultimate limit state (ULS), and verify the strength and stability resistance of each design.
- **Comparison:** evaluate the total amount of material used for both design methods.

Chapter 2

State of the art

This chapter will give an overview of the current state of concrete bridge design. As this thesis focuses on the quantitative difference in material use between conventional pedestrian bridges, constructed using tradition formworks, and form found concrete pedestrian bridges, cast using flexible formworks, Section 2.1 will discuss the design rules and considerations that are made for conventional concrete pedestrian bridges, as well as the standard fabrication process. With the existing demand for efficient and organic shaped structures, Section 2.2 explains how the shape finding process of form found concrete bridges takes place and how different types of formworks and additive manufacturing can be implemented into the fabrication process.

2.1 Conventional concrete pedestrian bridges

2.1.1 Design

Concrete bridges come in different shapes and sizes, depending on the function, location and crossing span. The majority of small modern bridges are simple reinforced solid slab concrete bridges. Solid slab bridges are the simplest form of reinforced concrete bridge structures. Their simplicity makes them the most economical solution for short spans (Parke et al., 2008). These bridges are most effective for spans of approximately 4 m to 8 m (American Association of State Highway and Transportation Officials., 2009). An example where this bridge-type is used is for typical pedestrian bridges as seen in Figure 2.1 These bridges are designed to carry primarily pedestrians, cyclists and light maintenance vehicles.

Figure 2.1 : An solid slab reinforced concrete pedestrian bridge in Malawi (Dennis, 2015)

The geometry of bridges is usually based on the known span-to-depth ratio for the chosen bridge type. The purpose of design calculations is ultimately only to design the reinforcement. A typical short span simply supported slab bridge has a span-to-depth ratio between 10-15. The appearance of these types of bridges is neat and simple. In terms of construction they require the simplest formworks and types of details (Clark et al., 1995; Parke et al., 2008).

2.1.2 Fabrication

Reinforced concrete structures are beloved for their simplicity; place a formwork, fix the reinforcement, pour concrete, and let it harden. The formwork is often made from timber (Figure 2.2a) and is used to give the structure its designed shape. The concrete gives the structure its compressive strength, while the reinforcement carries the tensile stresses caused by bending. (Parke et al., 2008). Normally reinforced concrete slab bridges are constructed in-situ. However, when the span is very short (i.e. less than 6 m) the prefabricated solution is more economical.

(a) (b)

Figure 2.2 : Two main types of formworks used for solid slab bridge designs: (a) timber formwork used for in-situ casting; (b) steel formwork used for prefabrication (photo credit: (a) De Boer & De Groot; (b) Cometal).

Important issues with the construction of bridges is the speed of construction, the fabrication costs and the hinderance of traffic during construction. Eurocode 2 defines precast structures as follows: “Precast structures are characterised by structural elements manufactured elsewhere than in the final position in the structure.” (Eurocode 2, 2004). Precast concrete manufacturing brings many potential advantages in quality control, construction speed and construction cost. The possibility to manufacture the concrete elements in a controlled environment, results in superior strength development, compared to on-site construction. This permits the use of thinner sections, resulting in significant material savings. Furthermore, the fact that no falsework is needed during construction makes it often the only construction option in densely populated regions, where the hinderance of

traffic is prohibited. Lastly, concrete plants make use of standardized (steel) moulds (Figure 2.2b) for the production of prefabricated concrete elements. This allows for them to be reused, which helps decrease the amount of construction waste.

2.2 Form found concrete pedestrian bridges

2.2.1 Design

Form finding is a progressive procedure whereby the design parameters of a structural design keep getting altered until the 'optimal' design is found that provides a state of static equilibrium for the given design load (Adriaenssens et al., 2014). The two main methods for form finding of shells are the physical form-finding methods and computational form-finding methods. Physical form-finding procedure often consists of hanging models or soap film models. There are many computational form-finding methods available; the main ones being the dynamic relaxation method, the force density method, the particle-spring system, topology optimization and shape optimization.

During hanging model experiments a chain or flexible membrane is subjected to a form determining load case. As a result of the loading, the chain/membrane follows a certain shape that is characterized by pure tension and no bending. When the shape is inverted it gives the shape for a shell with a pure compression stress state. Famously, Gaudi has used the hanging model principle for the design of the Sagrada Familia in Barcelona (Figure 2.3a-c). Similarly Heinz Isler (Figure 2.3b-d) has used this method to create successful and economical shell structures.

(a)

(b)

(c)

(d)

Figure 2.3: (a) Recreation of Gaudi's hanging model for the Sagrada Familia; (b) Isler's hanging model for one of his experiments; (c) Columns of the Sagrada Famalia by Gaudi, Barcelona, Spain ; (d) Service Station concrete shell structure by Heinz Isler, Deitingen, Switzerland, 1968 (photo credit: (a) Dan Scorpio; (b) Chilton pp. 37; (c) SBA73 (d) Nicolas Janberg).

A soap film creates a minimal surface, characterized by the fact that:

1. It locally minimizes its area;
2. The area is constant;
3. It has the same stresses in all directions; and
4. It has zero mean curvature.

Characteristically for soap film, as a result of surface tension, is that its surface area is minimized. Soap films find the optimal equilibrium shape of a minimal surface between the pre-set (closed) boundaries. Similarly, membrane structures and shells, usually only require the minimal surface between set boundaries to be found. Form finding a fabric structure with a soap film or minimal surface is done by setting the membrane stress (σ) components:

$$\sigma^{\alpha\beta} = Tg^{\alpha\beta} \qquad \text{(Eq. 2.1)}$$

T: $surface\ tension$

g: $mesh\ conditions$

α: $\alpha\ factor$

β: $\beta\ factor$

An example of a concrete bridge structure that was realized using a soap film model (Figure 2.4a) was Sergio Musmeci's Basento bridge (Figure 2.4b). The bridge consists of a slender continuous shell structure that serves as the load-bearing system and is loaded by uniform anisotropic compressive membrane stresses. The shape of the shell is based on the principle of minimal surfaces, which is then inverted to form a structure that is loaded by compression.

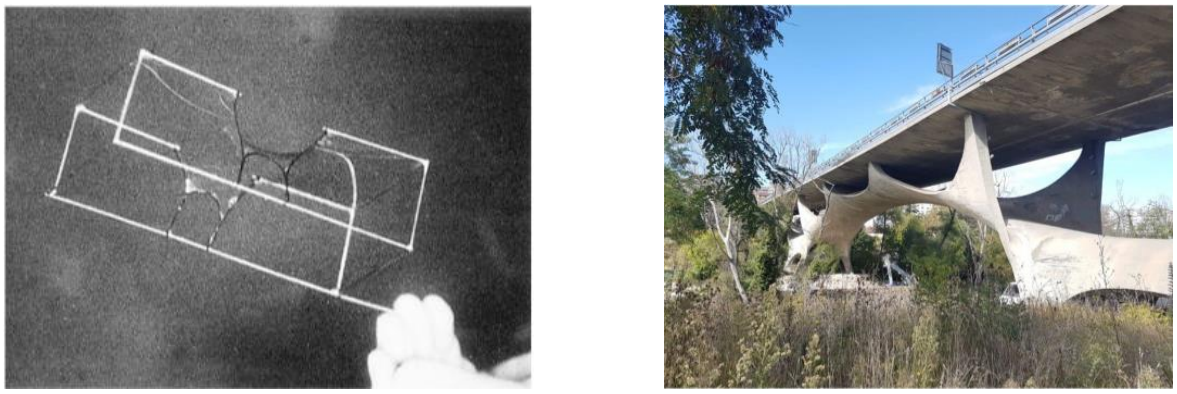

(a) (b)

Figure 2.4 : (a) Soap film model for the Basento bridge; (b) Basento bridge by Sergio Musmeci,1976 (photo credit: (a) Fenu, et al, 2020; (b) Carlo Atzeni).

The dynamic relaxation method is used to find the shape of net and membrane structures, by letting the structure relax to an equilibrium situation. The structure is modelled as a system of nodes, which are connected by members. The stiffness of each node depends on the strain of each member. Dynamic relaxation has an iterative, converging process where in the end an equilibrium should be reached. On one hand, the velocity of displacement converges to zero and the stiffness of the structure increases. An advantage of this method over matrix methods is that this method does not have to solve matrices, which decreases the calculation time. Another benefit is the ability to deal with local instabilities, like wrinkling of the membrane. The dynamic relaxation method has been used for the form-finding of a suspension bridge (Segal et al., 2015), a shallow arch (Halpern & Adriaenssens, 2015), and tensegrity bridges (Rhode-Barbarigos et al., 2010).

The force density method (FDM) uses an analytic technique to linearize the form-finding equation for a tension net. The force density ratios (cable force divided by cable length) are specified for each element. Different ratios provide different equilibrium shapes. This implies, the higher the force density, the shorter the element for a given force. When the force densities for a node are equal and evenly distributed around the node, a minimal surface (i.e. equilibrium shape) is generated. The method is independent of the initial locations of the nodes, numerically robust, and the equilibrium shape can be obtained easily. Furthermore, the linearization makes the method independent of the material properties of the membrane. To generate the 3D geometries of suspension bridges and arches, Descamps et al. (2011), used the FDM. Caron et al. (2009) used this method to balance stress levels in the hanger attached to a rigid bowstring. Quagliaroli and Malerba (2013) used an advanced version of this method to develop flexible bridge decks suspended by cable nets.

Particle-spring systems consist of lumped masses, called particles, which are connected by linear elastic springs. Each of the mass-less springs is assigned a constant axial stiffness, an initial length, and a damping coefficient. Springs generate a force when displaced from their rest length. Each particle in the system has a position, a velocity, and a variable mass, as well as a summarized vector for all the forces acting on it. The gravitational pull on a particle causes it to displace and subsequently stretch the springs it is attached to. The particle continues displacing until the sum of the spring forces matches the downward force of the mass the particles. This occurs to every particle until eventually the entire system reaches a state of equilibrium. This form-finding method was used to determine the shape of the shell-supported footbridge by Fenu et al. (2020) (Figure 2.5).

(a) (b)

Figure 2.5: (a) Form found shape of the load-bearing shell structure; (b) Shell-supported footbridge design (photo credit: Fenu et al., 2020).

The purpose of topology optimization is to find the optimal layout of a structure within a specified domain. The algorithm computes a structural layout that performs the best for the given inputs (i.e. applied loads, support conditions, volume of the structure, prescribed holes, etc.). For the post-tensioned 3D-printed concrete bridge realized by Ghent University and Vertico (Figure 2.6), the form was obtained by simultaneously optimizing the shape of the prestressing tendons and the topology of surrounding concrete (Amir & Shakour, 2018; Vantyghem et al., 2020). Fauche et al., (2010) used topology optimization to obtain the design of a thin-shell bridge structure (Figure 2.7). The topology optimization algorithm computed the material distribution that resulted in the maximum overall stiffness for a given volume of material.

(a) (b)

Figure 2.6 : (a) The principal stress plots for optimized layout with T_{pre} = 0.8 x T_{STD}; (b) The resulting post-tensioned 3D-printed concrete bridge (photo credit: (a) Amir & Shakour, 2018; (b) Vantyghem et al., 2020)

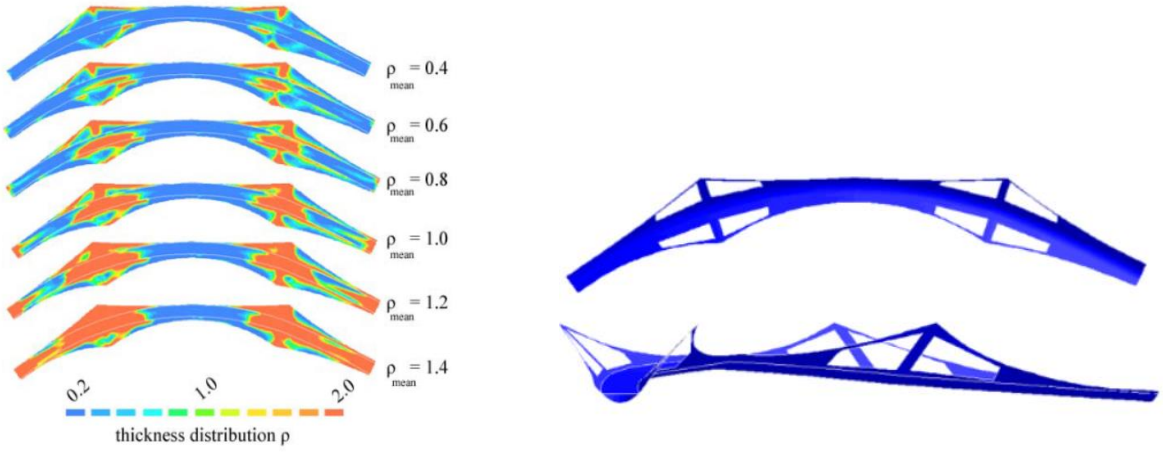

(a) (b)

Figure 2.7 : (a) The principal stress plots for optimized layout with T_{pre} = 0.8 x T_{STD} (Amir et Shakour, 2017); (b) The resulting post-tensioned 3D-printed concrete bridge (Vantyghem, et al., 2020).

The aim of shape optimization is to find the geometry that results in maximum performance of the structure. During the optimization the topology of the domain is fixed, but the domain boundaries are design variables. Salet et al. performed a shape optimization during the upscaling process of the 3D printed cycling bridge. The objective of the optimization was to reduce the printing path length. The shape optimized final design (Figure 2.8a) saved 4% of the printing path length compared to the 1:2 scale model for testing (Figure 2.8b) (Salet et al., 2018).

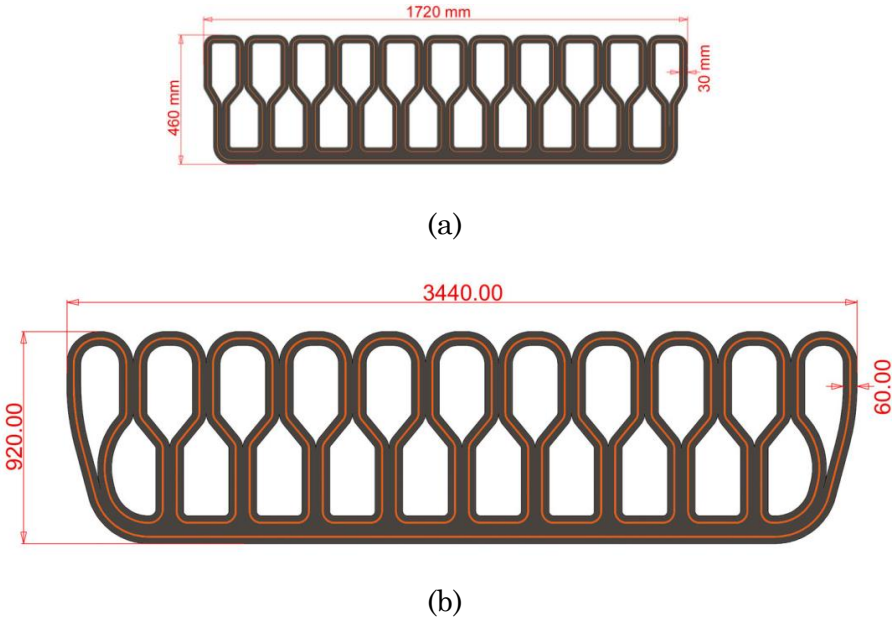

Figure 2.8 : (a) print paths of the 1:2 scale model for testing; (b) optimized pattern of the final bridge section (Salet et al., 2018).

2.2.1 Fabrication – formworks

Concrete is a favourable material for double-curved structures like shells, due to its ability to be moulded in any desired shape. However, it is not efficient to cast such complex shapes using traditional formworks that can only be used once. There is demand for more efficient methods.

A commonly used type of formwork for the production of curved surfaces are digitally fabricated timber formworks. These formworks can either be thin CNC-cut timber (plywood) plates (Figure 2.9a) or CNC-milled moulds (Figure 2.9b). The first type of formwork is often used in combination with a falsework to cast entire concrete structures, like ZJA's Extended Waalbridge in Nijmegen (Figure 2.10a). The CNC-milled moulds are used to create single concrete elements, like the façade elements of Grimshaw's Elizabeth Line (Figure 2.10b). Both formwork types are capable of producing single and double curved surfaces. In order to obtain a smooth surface, an additional finishing layer on top of the timber is sometimes necessary. However, this often limits the possibility of reusing the formwork.

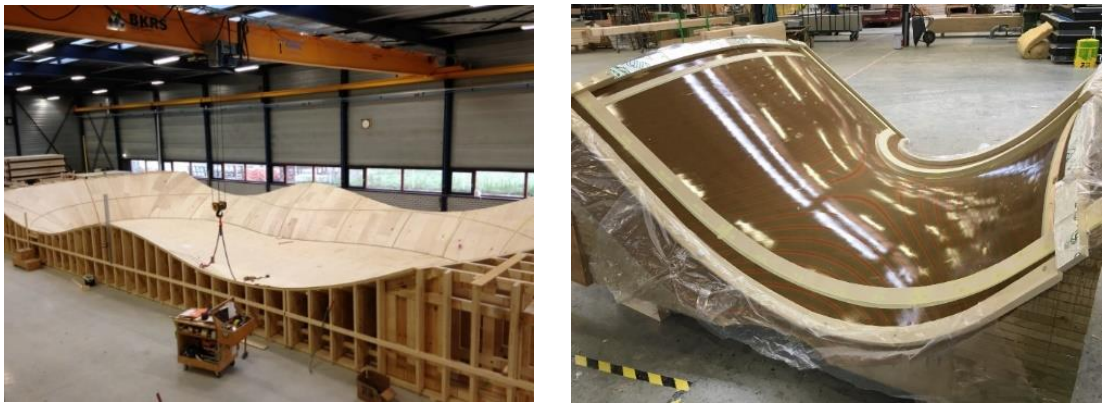

(a) (b)

Figure 2.9 : The two types of digitally fabricated timber formworks excecuted by Verhoeven: (a) the thin plate formwork and additional falsework for The Extended Waalbridge; (b) mould used to fabricate one of the concrete façade elements of The Elizabeth Line (photo credit: (a) Betoniek; (b) Verhoeven).

(a) (b)

Figure 2.10 : (a) The Extended Waalbridge by ZJA, Nijmegen, The Netherlands, 2015; (b) The Elizabeth Line by Grimshaw, London, United Kingdom, 2019; (photo credit: (a) Raymond van der Hoogt; (b) Grimshaw).

Another category of formworks that is used in the building industry, are CNC-milled foams. The foams that are mostly used are Expanded Polystyrene (EPS), Extruded Polystyrene (XPS) and Polyurethane (PU). Even though CNC-milling foams has the advantage of producing high precision details, it is also very time-inefficient, as the material removal using milling takes much time. A possible solution for this problem is by initially use hot wire cutting to remove a large bulk of the excess material before starting the CNC-milling. Usually after the CNC-milling is done, the foam is coated with a synthetic resin, like Polyurea. Once the polymer has hardened it is polished to finalize the process. The subtractive nature of CNC-milling of foams and the limited reusability of the moulds, causes this category of formworks to be considerable wasteful.

(a) (b)

Figure 2.11 : Examples of shell structures achieved by spraying concrete onto a pneumatic formwork: (a) the Bubble Houses by Wallace Neff, Pasadena, California, U.S.A., 1946; (b) the Balz House by Heinz Isler, Stetten, Germany, 1980 (Balz, 2022) (photo credit: (a) Jeffrey Head).

One technique that tackles the waste problem, which is characteristic for the subtractive methods, is the use of inflatable textiles as formwork. Many architects and structural engineers in the past and future have made use air pressure to construct these so called pneumatic concrete structures. The first iterations of this type of structures was realized by spraying concrete onto a pneumatic formwork. Some examples that used this method are the Bubble Houses in Pasadena by Wallace Neff (Figure 2.11a) (Neff, 1941) and Isler's Balz House in Stuttgart (Figure 2.11b). The second type of pneumatic structures first lets the concrete harden before the formwork is inflated. Once the structure has its final shape the gaps that have emerged due to the inflation process are filled with in-situ concrete. This method has lately started to get more attention, with new research being done by Kromoser and Kollogger at the Vienna University of Technology (Figure 2.12) (Kromoser & Kollegger, 2014). A drawback of this type of formwork, is that it is only capable of creating synclastic structures (i.e. structures with a positive Gaussian curvature).

Figure 2.12 : Experiment on pneumatic forming of hardened concrete at the Vienna University of Technology (Kromoser & Kollegger, 2014)

Another way of constructing form found structures, is by dividing them into multiple segments, which form a modular system. Hereby, each segment is a concrete element that is created using an adaptive mould. Subsequently, the elements are assembled on-site to form the final shell structure. Studies have shown that adaptive moulds are capable of creating double-curved elements (Grünewald et al., 2015; Raun & Kirkegaard, 2015; Schipper et al., 2015). There have even been some commercial applications of this method (Adapa, 2022; Hoppermann et al., 2015; Kristensen & Raun, 2011; Vollers & Rietbergen, 2009). Adaptive moulds work according to the following step-by-step plan (Figure 2.13a):

1. The mould, made form a flexible material (e.g. silicone), is supported by a subsystem that determines the desired final shape.
2. The mould is then filled with self-compacting concrete (SCC), which can be reinforced using fibres or textile reinforcement.
3. The SCC hardens for a short period of time in the flat position to obtain initial binding and stiffening. This prevents the concrete from flowing during the deformation process.
4. Next, the mould is carefully deformed into its desired final shape.
5. The concrete is then allowed to further harden until it reaches its ultimate strength.
6. Finally, the (double-)curved panel is demoulded and the mould can be re-used to create the next (double-)curved panel (Schipper et al., 2015).

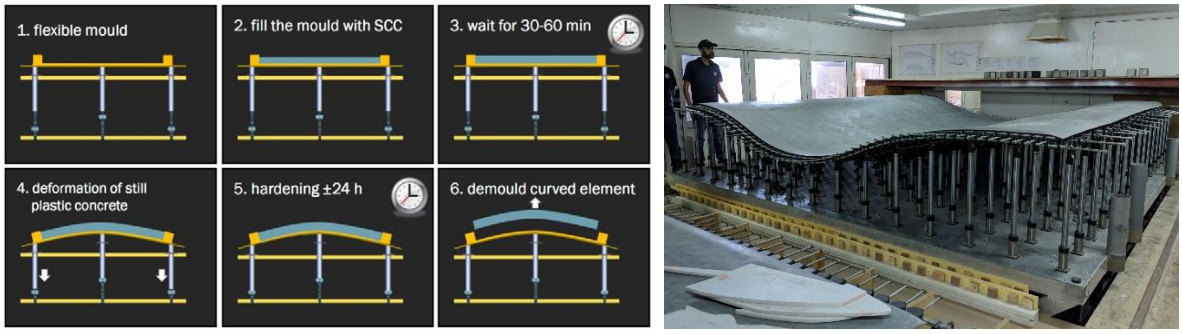

(a) (b)

Figure 2.13: (a) the manufacturing steps for a curved element using an adaptive mould according to (Schipper et al., 2015): (1) flexible mould in flat state; (2) flexible mould filled with SCC; (3) first hardening stage; (4) gradual deformation towards desired shape; (5) second hardening stage; (6) demoulding of curved element; (b) Adapa D300 adaptive mould (Adapa, 2022)

Adaptive moulds are advantageous with regards to reusability and the ability to produce both synclastic and anticlastic elements. However, the technique is limited in terms of the geometric freedom, as it can only produce panels with limited curvature. Furthermore, the process requires deformation of the concrete during its hardening period. The strains that result from these imposed deformations can negatively affect both the structural strength

of the panels, as well as the appearance of the panels, for example because of the presence of wrinkles and/or cracks.

Recently, a new formwork technology has been developed called KnitCrete (Popescu, 2019). KnitCrete makes use of 3D weft-knitted textiles as flexible and cost-effective stay-in place formwork. Knitted textiles have the advantage that they can be tailored to complex 3D shapes, allowing them to contain special features like channels, holes spacers, ribs and pockets, without the need of glue or the presence of seams. Furthermore, it allows for custom placement of material and surface texturing, which helps control the performance of the formwork during the construction. A computational pipeline is used to transform the designed 3D geometry into a printing pattern. This printing pattern can then be shared with CNC knitting machines available anywhere around the world. The final product is a lightweight knitted textile that can be easily compacted and transported to the construction site. At the construction site the textile is tensioned to obtain its desired shape. Next, a thin layer of a special adhesive or cement-paste is spayed on top of the fabric to stiffen it and make it the basis of the concrete structure. Lastly, the structural concrete is applied manually to finish the shell.

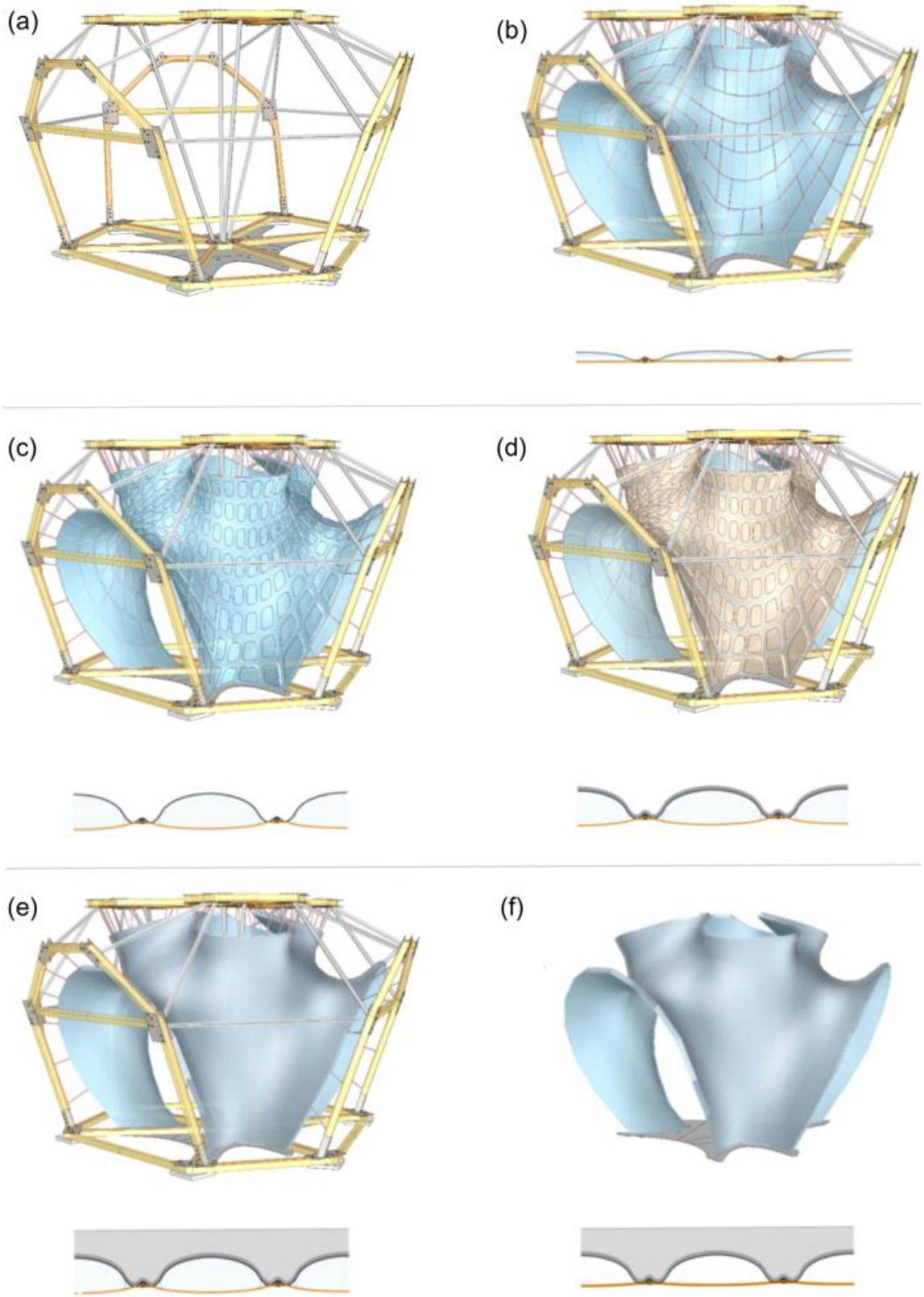

Figure 2.14 : Construction process of the KnitCandela: (a) external frame; (b) tensioned knit; (c) inflated pockets; (d) initial cement-paste layer; (e) structural concrete; (f) final structure (Popescu, 2019)

2.2.1 Fabrication – additive manufacturing

Even though formworks determine the shape of the structure, they are limited in defining the material placement in the structure. This is where another fabrication method, that can be used to create free form structures, is introduced: additive manufacturing. The two approaches of additive manufacturing of concrete structures that are mentioned in this paragraph are extruded 3D concrete printing (E3DCP) and shotcrete 3D printing (SC3DP).

E3DCP is the most popular concrete additive manufacturing method in the construction industry to date. During the printing process the concrete gets extruded in continuous strands that are layered on top of each other to form the structure (Figure 2.15a). Once the cementitious material reaches the print head, it is squeezed through the nozzle to form a filament with a certain shape, depending on the chosen nozzle type. The cycling bridge by the TU Eindhoven consists of six 3D printed elements, produced using E3DCP that are bonded by prestressing (Salet et al., 2018). The cross-section of the bridge elements consists of a series of connected bottle shapes, alternatively positioned upside down, in combination with a continuous connecting straight line at the bottom (Figure 2.8b).

(a) (b)

Figure 2.15 : (a) extruded 3D concrete printing; (b) the 3D printed cycling bridge by TU Eindhoven; (photo credit: (a) Houben/Van Mierlo architects; (b) Salet et al, 2018).

Before each layer of extruded concrete is covered by the next, there is a delay. This delay causes 'cold joints', which are weaker bonds between two adjacent layers (Hack & Kloft, 2020). The interlayer bond strength is highly reliant on adhesion, which is a function of the delay time between the deposition of two subsequent layers. By decreasing the time interval between each extrusion, the degree of adhesion increases. However, this also causes the previous layer to not cure sufficiently. This results in the bottom layer no having enough strength to carry the top layer, which negatively affect the buildability (Wolfs et al., 2019). This phenomenon of cold joints has a negative impact on the mechanical properties of structures, made using this additive manufacturing method.

During shotcrete 3D printing (SC3DP) the concrete is sprayed with pressure to create the 3D structure (Figure 2.16a). Spraying a dispersed stream of concrete promotes several distinct features:

- Mechanical layer intermixing, resulting in an intense layer bond
- The concrete flows around the structural reinforcement, which helps to embed it
- It allows the creation of pronounces overhangs by gradually transitioning from the horizontal printing plane to the vertical printing plane.
- It makes it possible for the concrete to adhere to vertical surfaces. This makes it possible to spay a secondary layer onto the vertical surface, which subsequently can be smoothed automatically using a robot, like shown during the fabrication process of the double curved wall (Figure 2.16b), produced in the Digital Building Fabrication Laboratory (DBFL) of the Technical University of Braunschweig (Kloft et al., 2020).

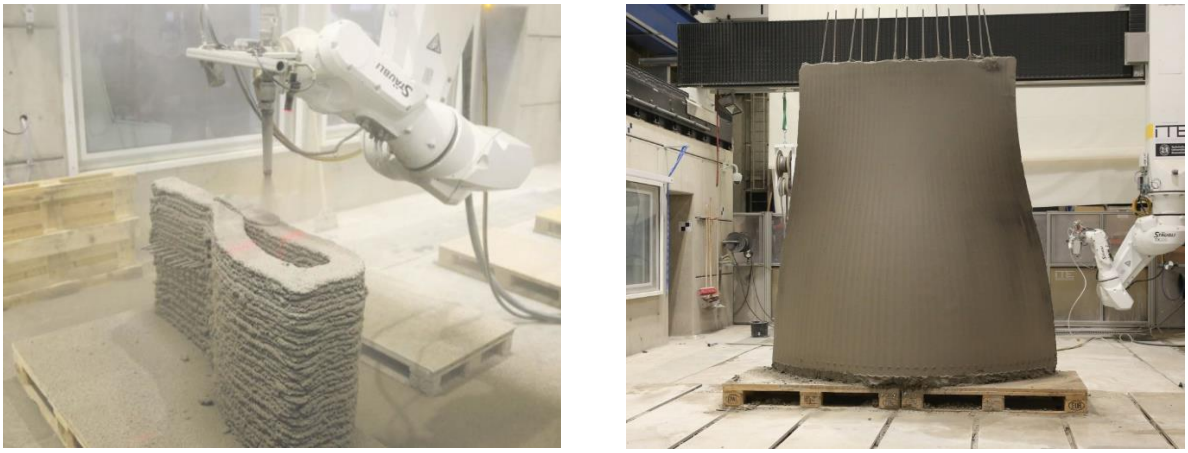

(a) (b)

Figure 2.16: (a) Shotcrete 3D printing in the Digital Building Fabrication Laboratory at TU Braunschweig; (b) Double curved wall fabricated in the Digital Building Fabrication Laboratory at TU Braunschweig (photo credit: ITE, TU Braunschweig).

Studies have shown that SC3D printed specimen have higher bulk densities compared to conventional 3D printed samples. The higher bulk density of the SC3D printed elements is a result of compaction due to the high kinetic energy during spraying. As a result of the higher bulk density SC3D printed samples have a higher compressive and flexural strength compared to the extruded samples. The excellent mechanical properties of SC3D printed specimen can mainly be attributed to the enhanced interlocking. As the concrete is sprayed it creates a concrete layer with a high surface roughness. This induces inter-locking between the spayed layer, which enhances the splitting tensile and compressive strength (Kloft et al., 2020).

The SC3DP process generally allows for material deposition either in linear layers (Figure 17a), or with overlapping rotational movement (Figure 17b) as well as building-up elements with varying angles (Figure 17c). The layer thickness can be controlled by the robot speed (path velocity) (Figure 17d), whereas the layer width can be adjusted by varying the nozzle distance from the surface (Figure 17e). In addition, the application process can be actively controlled by comparing the printed with the nominal values based on in-situ measurements of the applied layer geometry (distance and width) (Figure 17f) (Kloft et al., 2020).

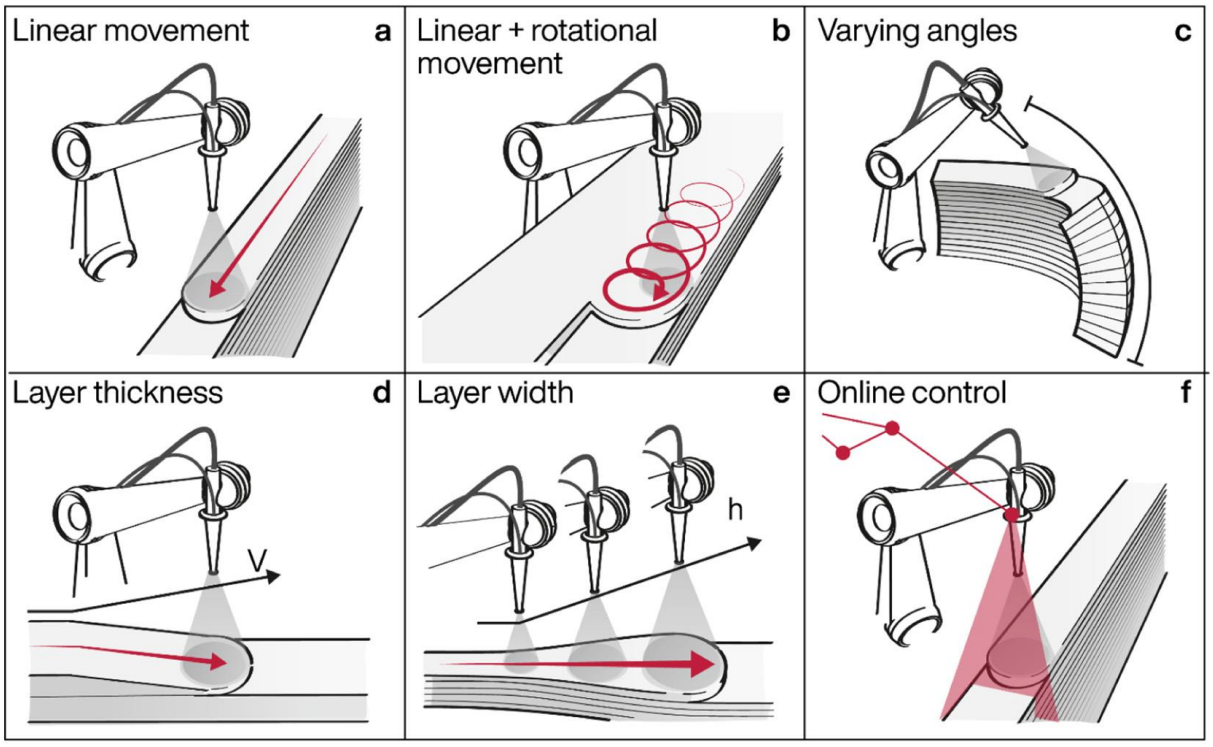

Figure 2.17 : Specific deposition methods of the SC3DP process: (a) layer-by-layer deposition; (b) laminar application; (c) variation of application angle; (d) control of layer thickness by robot speed *(V)*; (e) control of layer width by nozzle distance *(h)*; (f) line laser for in-situ measurement of layer distance and width (Kloft et al., 2020).

2.3. Summary

The two types of bridge designs presented in this chapter are based on different design philosophies. The conventional solid slab bridge design is based on rules of thumb, which have been verified by years of experience. The design is conservative, which gives the bridges based this design their robustness and neat appearance. The form found bridge design uses physical or computational form-finding methods to obtain a shape that corresponds with the governing load case(s). The design takes advantage of the mouldability of concrete to create organic shells that are both efficient and elegant looking.

The fabrication process of conventional bridges has cemented itself over the years, whereas the fabrication process of shell structures still has a lot of room for innovative methods. In terms of formworks, KnitCrete addresses both the problems of construction waste and geometric freedom effectively. The lightweight knitted textile requires minimal amount of external formwork to tension it into its final shape. By integrating SC3DP with KnitCrete it offers the additional option to apply concrete specifically at the locations where it is needed.

Chapter 3

Methodology

3.1 Design

3.1.1 Context

For this study, multiple concrete pedestrian bridges will be designed using the conventional and the form found concrete design approaches. Since most pedestrian bridges with spans up 45 meters can be prefabricated and transported as one piece (Pipinato, 2022) the bridges will be designed for spans of 5 m, 10 m, 20 m and 45 m. All designs will have a width of 2 meters at the supports.

3.1.2 Conventional concrete pedestrian bridge

As mentioned in Chapter 2, the height of the conventional concrete pedestrian bridge is determined by the span-to-depth ratio. In the case of a conventional concrete pedestrian bridge, the ratio is between 10 and 15.

In order to minimize bias during the design process a reference concrete bridge design is used (Childs, 2020). Table 3.1 gives the predetermined design properties obtained from the reference design.

Properties	
Steel strength class	B500
Maximum water-cement ratio	0.55
Minimum cement content	320 kg/m^3
Concrete density (γ_{conc})	25 kN/m^3
Concrete coverage (c_{nom})	60 mm (Eurocode BS 8500-1 Table A.5)

Table 3.1. Predetermined properties of the conventional concrete pedestrian bridge designs (Childs, 2020)

The concrete class, rebar diameters and rebar spacing, will be altered for each design in order to obtain the most efficient structures.

3.1.3 Form found concrete pedestrian bridge

The initial geometries of the form found concrete pedestrian bridge designs are obtained using the Rhinoceros form finding plug-in Kangaroo. Once the anchorage points of the supports are selected and the loading direction is given, the form finding process can be initiated. The result of the Kangaroo form finding procedure is an arch shaped structure that narrows down towards the midspan (Figure 3.1).

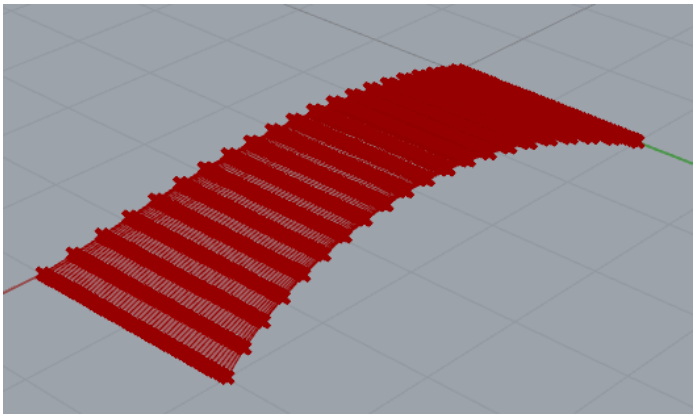

Figure 3.1. Initial footbridge geometry resulting from the Kangaroo form finding process

Subsequently, the knitted formwork is modelled. First, the four bending active ribs are modelled and parametrized using NURBS curves. The midspan height, span, angle and spacing of the curves can be altered. This parametrization will be used during the shape optimization procedure. Next, a custom Grasshopper function is used that models the shape of the prestressed knitted formwork (Figure 3.2).

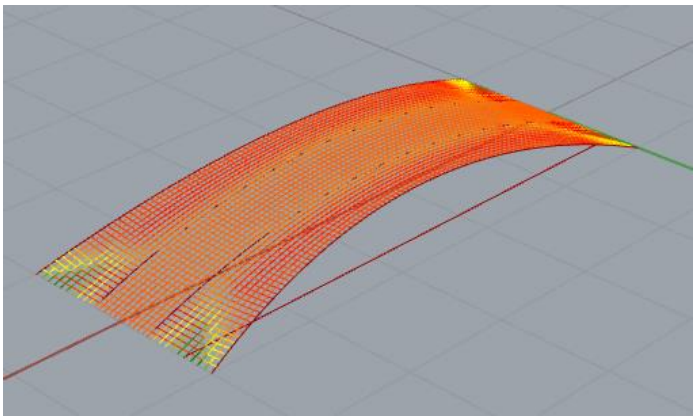

Figure 3.2. Model of the prestressed knitted formwork

For the shape optimization process the Rhinoceros plug-in Opossum is used. The midspan height, span, angle and spacing of the curves are chosen as variables. The objective is to minimize bending action. Some functional requirements were added to make the bridges usable:

- The ramp slope should be within the ideal grade interval of 1:20 to 1:12 (British Standards Institution, 2018)
- The path width should be larger than 1.50 meters in order to allow two users to pass each other.

The final optimized shape of the form found pedestrian bridge designs (Figure 3.3)

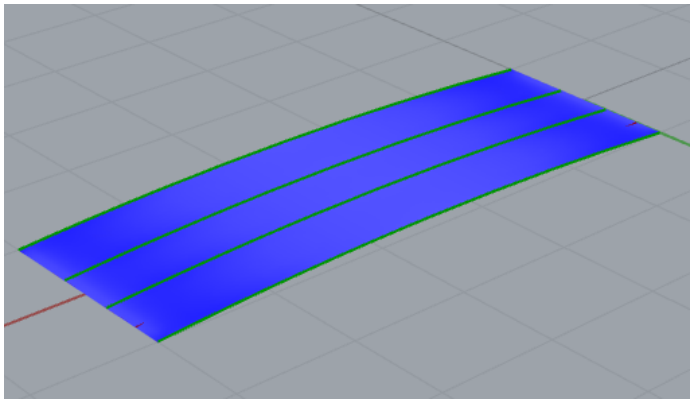

Figure 3.3. Model of the prestressed knitted formwork

Similar to the convention concrete pedestrian bridge design, the concrete class and concrete thickness can be altered to realize efficient designs. However, in order to compare the material-use of the two design types for a certain span, the form found concrete footbridge design uses the same concrete class as the conventional concrete footbridge design. Furthermore, the use of SC3DP for the form found footbridge design allows for variation of the concrete thickness over the span of the bridge. This feature is used to minimize internal forces and bending moments caused by self-weight.

3.2 Calculation

The design calculations for both bridge types are for a 1 metre width of deck (i.e. unit strip method). This method was also used in the reference design calculations of Childs (2020). Furthermore, this method is also used in the finite element analyses (FEA) performed in Karamba3D.

The calculations are performed for three governing cases:

- **Fully loaded vertically**: the structural strength is examined for the situation in which the entire surface of the pedestrian bridge is exposed to the vertical design load.
- **Asymmetrically loaded vertically**: the structural strength is examined for the situation in which only half of the structure is exposed to the vertical design load.
- **Buckling**: the structural stability is examined for the governing axial compression force.

3.2.1 Conventional concrete pedestrian bridge

The first step is to define the loads that act on the bridge. For the conventional concrete pedestrian bridge designs the permanent loads (G_k) are obtained using EN 1991-1-1 Annex A. The variable loads (Q_k) are obtained using EN 1991-2 cl. 4.3.5. For pedestrian bridges Q_k is equal to 5 kN/m^2. Next a combination of actions is considered for the ultimate limit state (ULS):

$$Q_{ULS} = \gamma_{Gj} G_{kj} + \gamma_{Q1} Q_{k1} \quad \text{(Eq. 3.1)}$$

$G_{kj}: permanent\ loads$

$Q_{k1}: variable\ loads$

$\gamma_{Gj}: safety\ factor\ for\ permanent\ loads$

$\gamma_{Q1}: safety\ factor\ for\ variable\ loads$

The safety factors used in Eq. 3.1 are given in Table 3.2.

	Value
Permanent loads (γ_{Gj})	1.35
Variable loads (γ_{Q1})	1.5

Table 3.2. Safety factors for different loading groups, according to Eurocode 2 Part 2 Table NA.A.2.4

Now that the design load has been determined the next step is to examine the performance of the structure using the unity checks (UC). First, the bridge is tested for bending moment action. The governing bending moment is calculated for the full vertical load case and asymmetric vertical load case using the following equation:

$$M_{Ed,full} = \frac{1}{8} Q_{ULS} l^2 \quad \text{(Eq. 3.2)}$$

$$M_{Ed,asym} \approx \frac{13}{136} Q_{ULS} l^2 \quad \text{(Eq. 3.3)}$$

$l: length\ of\ the\ bridge$

Next, the bending moment resistance of the footbridge is using the following formulae:

$$M_{ult} = f_{av} bxz = f_{av} bx(d - \beta x) \quad \text{(Eq. 3.4)}$$

$f_{av}: average\ concrete\ strength$

$b: width\ of\ the\ bridge$

$x: height\ of\ the\ compression\ zone$

$z: internal\ lever\ arm\ height$

$d: total\ height\ of\ the\ bridge$

$\beta: reduction\ factor$

$\gamma_s = 1.15\ and\ \gamma_c = 1.5\ (Table\ 2.1N),\ \ a_{cc} = 1\ (cl. 3.1.7)$

$$f_{av} = \frac{a_{cc} f_{ck}}{\gamma_c} \left(1 - \frac{\varepsilon_{c2}}{\varepsilon_{cu2}(n+1)}\right) \quad \text{(Eq. 3.5)}$$

$$\beta = 1 - \left(\frac{(0.5\varepsilon_{cu2}^2 - \varepsilon_{c2}^2)(n+1)}{(n+1)(n+2)(\varepsilon_{cu2}^2 - \varepsilon_{cu2}\varepsilon_{c2})}\right) \quad \text{(Eq. 3.6)}$$

$$x = \frac{f_{yk} A_s}{f_{av} b \gamma_s} \quad \text{(Eq. 3.7)}$$

Table 3.3 gives the deformation characteristics that are required to solve Eq. 3.6.

	ε_{cu2}	ε_{c2}	n
C12/15 – C50/60	0.0035	0.002	2
C55/65	0.0031	0.0022	1.75
C60/75	0.0029	0.0023	1.6
C70/85	0.0027	0.0024	1.45
C80/95	0.0026	0.0025	1.4
C90/105	0.0026	0.0026	1.4

Table 3.3. Deformation characteristics for different concrete classes, according to Eurocode 2 Part 2 Table 3.1

Note: Eq. 3.4 can only be used to calculate the bending moment resistance, if the steel yields: $\varepsilon_s > \varepsilon_{s,yield}$. To check whether this is the case, the following equations can be used:

$$\varepsilon_{s,yield} = \frac{f_{yk}}{E_s \gamma_s} \quad \text{(Eq. 3.8)}$$

$\varepsilon_{s,yield}$: $steel\ strain\ at\ point\ of\ yielding$

f_{yk}: $characteristic\ yield\ strength\ of\ steel$

γ_s: $safety\ factor\ of\ steel$

E_s: $elastic\ modulus\ of\ steel$

$$E_s = 200 \frac{kN}{mm^2}\ (cl.\ 3.2.7(4))$$

$$\varepsilon_s = \varepsilon_{cu2}\left(\frac{d}{x} - 1\right) \quad \text{(Eq. 3.9)}$$

ε_s: $steel\ strain$

ε_{cu2}: $ultimate\ concrete\ strain$

Next, the bridge is tested for shear force action. The governing shear force is calculated according to EN 1992-1-1 Cl. 5.4.4. The formulae for the governing shear force for the full vertical load case and asymmetric vertical load case are:

$$V_{Ed,full} = \frac{1}{2} Q_{ULS} l \quad \text{(Eq. 3.10)}$$

$$V_{Ed,asym} \approx \frac{7}{16} Q_{ULS} l \quad \text{(Eq. 3.11)}$$

Q_{ULS}: $ultimate\ limit\ state\ load$

The shear force capacity of the slab is determined using EN 1992-1-1 Cl. 6.2.2(101):

$$V_{Rd,c} = \left[C_{Rd,c} k (100 \rho_1 f_{ck})^{1/3}\right] b_w d \quad \text{(Eq. 3.12)}$$

$C_{Rd,c}$: $shear\ force\ resistance\ constant$

k: $k\ factor$

ρ_1: $reinforcement\ ratio$

f_{ck}: $characteristic\ concrete\ compressive\ strength$

b_w: $width\ of\ the\ bridge$

d: $total\ height\ of\ the\ bridge$

$$C_{Rd,c} = \frac{0.18}{\gamma_c} = \frac{0.18}{1.5} = 0.12$$

γ_c: $safety\ factor\ of\ concrete$

$$k = 1 + (\frac{200}{d})^{0.5} \leq 2.0 \quad \text{(Eq. 3.13)}$$

$$\rho_1 = \frac{A_{s1}}{b_w d} \leq 0.02 \quad \text{(Eq. 3.14)}$$

The minimum shear force capacity is checked using EN 1992-1-1 Cl. 3.1.2(102)P:

$$V_{Rd,c,min} = (v_{\min}) b_w d \quad \text{(Eq. 3.15)}$$

$$v_{\min} = 0.035 k^{3/2} f_{ck}^{1/2} b_w d \quad \text{(Eq. 3.16)}$$

$v_{\min}$: $minimum\ unit\ shear\ strength$

Lastly, the maximum allowable shear force is calculated using EN 1992-1-1 Cl. 6.2.2(6):

$$V_{Rd,c,max} = 0.5\ b_w d v f_{cd} \quad \text{(Eq. 3.17)}$$

$$v = 0.6\left[1 - \frac{f_{ck}}{250}\right] \quad \text{(Eq. 3.18)}$$

v: $unit\ shear\ strength$

There is no axial compression force present in the convention concrete pedestrian bridge design, therefore, no need to check for buckling.

3.2.2 Form found concrete pedestrian bridge

The first step is to define the loads that act on the bridge. For the form found concrete pedestrian bridge designs the permanent loads (G_k) are obtained using the Loads function of Karamba3D, selecting load type "Gravity". The variable loads (Q_k) are obtained using EN 1991-2 cl. 4.3.5. Next a combination of actions is considered for the ultimate limit state (ULS) using Eq. 3.1. The safety factors used in Eq. 3.1 are given in Table 3.2.

The governing bending moment (M_{Ed}) and normal force (N_{Ed}) are obtained using the S-Force (Shell Section) function of Karamba3D. As a result of bending the top part of the shell will be loaded in compression and the top part in tension. Furthermore, the entire cross-section of the shell will be loaded by axial compression, due to the arch shape of the bridge. Therefore, governing stresses at the top and bottom of the shell are calculated using the following formulae:

$$\sigma_{top} = \left| -\frac{N_{Ed}}{bh} - \frac{M_{Ed}}{\frac{1}{6}bh^2} \right| \leq f_{cd} \quad \text{(Eq. 3.18)}$$

$$\sigma_{bottom} = \left| -\frac{N_{Ed}}{bh} + \frac{M_{Ed}}{\frac{1}{6}bh^2} \right| \leq f_{cd}\ (in\ the\ case\ of\ compression) \quad \text{(Eq. 3.19)}$$

$$\leq f_{ctk,0.05}\ (in\ the\ case\ of\ tension)$$

$$f_{cd} = \frac{a_{cc} f_{ck}}{\gamma_c} \quad \text{(Eq. 3.20)}$$

N_{Ed}: $design\ axial\ force$

M_{Ed}: $design\ bending\ moment$

h: $height\ of\ the\ bridge$

b: $width\ of\ the\ bridge$

f_{cd}: $design\ concrete\ compressive\ strength$

$f_{ctk,0.05}$: $characteristic\ 5th\ percentile\ concrete\ tensile\ strength$

Additionally, the utilization (i.e. the ratio between the strength of the material and maximum equivalent stress along the shell's cross-section) is checked using the Shell View function of Karamba3D. This is done to verify the calculations performed above.

The shear force check is the same as for the conventional bridge design.

Slender structures that carry loads mainly in compression, like shells, are susceptible to buckling. To determine whether the form found footbridge will fail due to buckling, the buckling load factor (BLF) must be calculated. The BLF is a multiplier of the largest applied axial compression force that causes the structure to buckle. In order for the structure to resist buckling, the buckling load factor has to be larger than 1. The structure has many buckling modes, however, the first buckling mode is analysed. This is the governing mode, as it requires the lowest force and therefore occurs first. The buckling load factor for the form found designs are calculated using the Buckling Modes function of Karamba3D.

3.3 Comparison

The final designs of the conventional method and form found method are compared for each span. Hereby, the amount of concrete, steel and textile for both design types are evaluated. This comparison process is performed for all three governing cases (full vertical loading, asymmetric vertical loading, buckling). The amount of concrete used in the form found designs is also expressed as a percentage of the amount of concrete used for the conventional design (in the remainder of this thesis it will be named “ratio”). This makes it possible to compare the efficiency of the designs for different spans and different load cases.

Chapter 4

Results and discussion

4.1 Calculation results

In the following paragraph the calculation results for the different conventional designs and form found designs are presented. The designs are examined for three governing states: fully loaded vertically, asymmetrically loaded vertically and buckling. The calculations were performed for different spans: 5 m, 10 m, 20 m and 45 m. Using an iterative process the properties of the designs were altered, until a sufficient design is obtained.

4.1.1 Full vertical loading

In this first load case the internal forces, bending moments and resulting stresses are determined for the situation, whereby the entire surface is loaded by the design load (Figure 4.1). For the conventional concrete footbridge designs the resistance to axial forces, shear forces and bending moments are determined and compared to the axial forces, shear forces and bending moments they are exposed to. For the form found concrete footbridge designs the governing stresses, resulting from bending and compression, are compared with the compressive and tensile strength of the concrete. A structure performs efficiently when the unity check (UC) values are close to, but not higher than 1.0 (i.e. 100% of the material contributes to carrying the load).

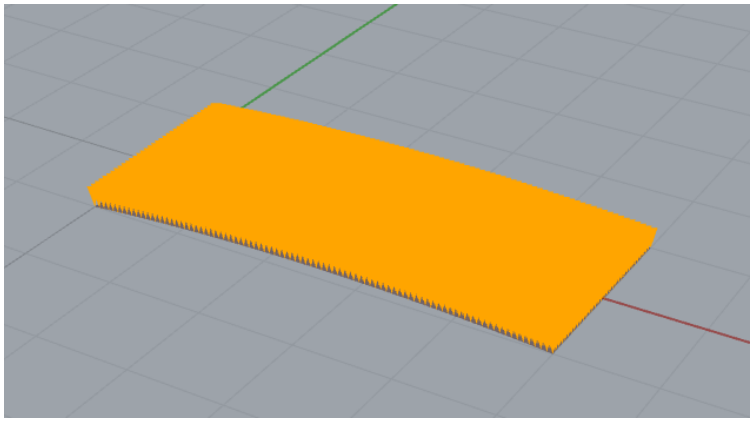

Figure 4.1: Fully vertically loaded case

Table 4.1 shows the calculation results of the conventional concrete footbridge designs for a span of 5 meters. For the final design, CSB_L5_V3, the bending moment resistance was governing, with an UC-value of 0.89.

	Properties				Shear force			Bending moment		
	d [mm]	Concrete class	Ø [mm]	s [mm]	V_{Ed} [kN]	V_{Rd} [kN]	UC	M_{Ed} [kNm]	M_{Rd} [kNm]	UC
CSB _L5_ V1	333	C12/15	8	333	45	52.72	0.85	56.25	17.08	3.29
CSB _L5_ V2	333	C20/25	12	250	45	89.82	0.50	56.25	49.36	1.14
CSB _L5_ V3	333	C40/50	12	200	45	121.9	0.37	56.25	63.21	0.89

**UC = Unity Check – ratio between design force/moment and resisting force/moment*

Table 4.1: Unity checks for the conventional concrete footbridge designs with a span of 5 m.

Table 4.2 shows the results of the design calculations of the form found concrete footbridge design. The design uses concrete of the same strength class as used for the conventional bridge design, C40/50, however the required thickness of the concrete is significantly lower, with a maximum thickness of 15 mm at the supports and minimum thickness of 10 mm at the midspan. The compressive stresses that occur at the bottom of the shell structure, due to bending and axial compression, are governing, with an UC-value of 0.90.

	Properties				Shear force		
	$d_{support}$ [mm]	$d_{midspan}$ [mm]	$h_{midspan}$ [mm]	Concrete class	V_{Ed} [kN]	V_{Rd} [kN]	UC
FFB_ L5_V	10	15	105	C40/50	1.39	28.34	0.05
	Bending + Normal stress (top)			Bending + Normal stress (bottom)			
	$\sigma_{Ed,top}$ [MPa]	f_{cd} [MPa]	UC	$\sigma_{Ed,bottom}$ [MPa]	f_{cd} [MPa]	UC	
	22.55	26.67	0.85	24	21.07	0.79	

**UC = Unity Check – ratio between design force/moment and resisting force/moment*

Table 4.2: Unity checks for the form found concrete footbridge design with a span of 5 m.

The additional utilization check (Figure 4.2) confirms the results given in Table 4.2, with a comparable value of 86.5 %. As can be seen in Figure 4.2, the entire structure acts in compression.

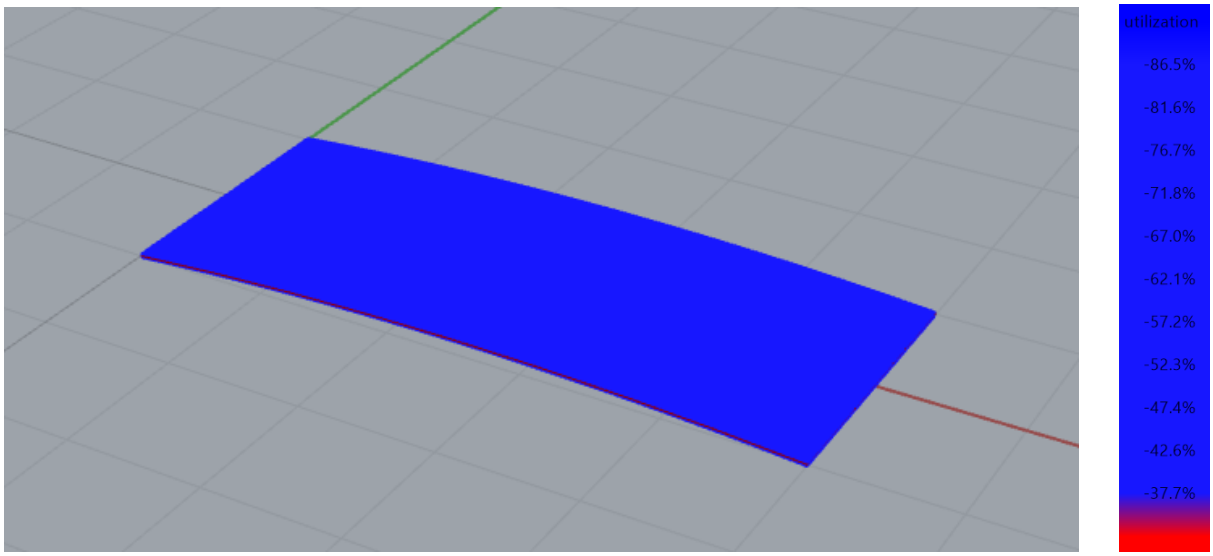

Figure 4.2: Contour plot of the 5 m long form found concrete footbridge illustrating the utilization rate (blue = compression, red = tension)

Table 4.3 shows the calculation results of the conventional concrete footbridge design for a span of 10 meters. For the final design, CSB_L10_V2, the bending moment resistance was governing, with an UC-value of 0.96.

	Properties				Shear force			Bending moment		
	d [mm]	Concrete class	Ø [mm]	s [mm]	V_{Ed} [kN]	V_{Rd} [kN]	UC	M_{Ed} [kNm]	M_{Rd} [kNm]	UC
CSB _L10 _V1	667	C50/60	14	200	146.3	211	0.69	365.6	197	1.86
CSB _L10 _V2	667	C50/60	18	167	146.3	264.5	0.55	365.6	381.3	0.96

**UC = Unity Check – ratio between design force/moment and resisting force/moment*

Table 4.3. Unity checks for the conventional concrete footbridge designs with a span of 10 m.

Table 4.4 shows the results of the design calculations of the form found concrete footbridge design. The design uses concrete of the same strength class as used for the conventional bridge design, C50/60, however the required thickness of the concrete is significantly lower, with a maximum thickness of 20 mm at the supports and minimum thickness of 15 mm at the midspan. The compressive stresses that occur at the top of the shell structure, due to bending and axial compression, are governing, with an UC-value of 0.96.

	Properties				Shear force		
FFB_ L10_V	$d_{support}$ [mm]	$d_{midspan}$ [mm]	$h_{midspan}$ [mm]	Concrete class	V_{Ed} [kN]	V_{Rd} [kN]	UC
	20	15	210	C50/60	1.32	37.24	0.04
	Bending + Normal stress (top)			Bending + Normal stress (bottom)			
	$\sigma_{Ed,top}$ [MPa]	f_{cd} [MPa]	UC	$\sigma_{Ed,bottom}$ [MPa]	f_{cd} [MPa]	UC	
	31.99	33.33	0.96	25.27	33.33	0.76	

**UC = Unity Check – ratio between design force/moment and resisting force/moment*

Table 4.4: Unity checks for the form found concrete footbridge design with a span of 10 m.

The additional utilization check confirms the results given in Table 4.4, with a comparable value of 95.3 %. The entire structure acts in compression.

As the spans increase in length, so does the required concrete strength. The elastic deformation characteristics of concrete change once the concrete strength is higher than C50/60. The concrete becomes more brittle as the strength class increases, which makes the structural resistance more depending on the steel reinforcement.

Table 4.5 shows the calculation results of the conventional concrete footbridge designs for a span of 20 meters. For the final design, CSB_L20_V2, the bending moment resistance was governing, with an UC-value of 0.96.

	Properties				Shear force			Bending moment		
	d [mm]	Concrete class	Ø [mm]	s [mm]	V_{Ed} [kN]	V_{Rd} [kN]	UC	M_{Ed} [kNm]	M_{Rd} [kNm]	UC
CSB _L20 _V1	1333	C60/75	18	100	517.5	489.5	0.69	2588	1365	1.86
CSB _L20 _V2	1333	C70/85	25	91	517.5	610.5	0.85	2588	2632	0.98

**UC = Unity Check – ratio between design force/moment and resisting force/moment*

Table 4.5: Unity checks for the conventional concrete footbridge designs with a span of 20 m.

Table 4.6 shows the results of the design calculations of the form found concrete footbridge design for a span of 20 m. The design uses concrete of the same strength class as used for the conventional bridge design, C70/85, however the required thickness of the concrete is significantly lower, with a maximum thickness of 25 mm at the supports and minimum thickness of 25 mm at the midspan. The compressive stresses that occur at the top of the

shell structure, due to bending and axial compression, are governing, with an UC-value of 0.95.

	Properties				Shear force		
FFB_ L20_V	$d_{support}$ [mm]	$d_{midspan}$ [mm]	$h_{midspan}$ [mm]	Concrete class	V_{Ed} [kN]	V_{Rd} [kN]	UC
	25	20	415	C70/85	1.37	49.73	0.03
	Bending + Normal stress (top)			Bending + Normal stress (bottom)			
	$\sigma_{Ed,top}$ [MPa]	f_{cd} [MPa]	UC	$\sigma_{Ed,bottom}$ [MPa]	f_{cd} [MPa]	UC	
	44.48	46.67	0.95	34.43	46.47	0.74	

**UC = Unity Check – ratio between design force/moment and resisting force/moment*

Table 4.6: Unity checks for the form found concrete footbridge design with a span of 20 m.

The additional utilization check confirms the results given in Table 4.6, with a comparable value of 87.5 %. The entire structure acts in compression.

During the calculation process, it could be concluded that spans longer than 20 meters are not achievable using the conventional concrete footbridge design. Longer spans require alternative construction methods, for example, ZIP-beams.

Table 4.7 shows the results of the design calculations of the form found concrete footbridge design for a span of 40 m. The design uses concrete with strength class C90/105. The required thickness of the concrete is largest at the supports with thickness of 45 mm and lowest at the midspan with a thickness of 40 mm. The compressive stresses that occur at the top of the shell structure, due to bending and axial compression, are governing, with an UC-value of 0.94.

	Properties				Shear force		
FFB_ L45_V	$d_{support}$ [mm]	$d_{midspan}$ [mm]	$h_{midspan}$ [mm]	Concrete class	V_{Ed} [kN]	V_{Rd} [kN]	UC
	45	40	940	C90/105	2.27	77.32	0.03
	Bending + Normal stress (top)			Bending + Normal stress (bottom)			
	$\sigma_{Ed,top}$ [MPa]	f_{cd} [MPa]	UC	$\sigma_{Ed,bottom}$ [MPa]	f_{cd} [MPa]	UC	
	56.12	60	0.94	50.96	60	0.85	

**UC = Unity Check – ratio between design force/moment and resisting force/moment*

Table 4.7: Unity checks for the form found concrete footbridge design with a span of 45 m.

The additional utilization check confirms the results given in Table 4.7, with a comparable value of 93.7 %. The entire structure acts in compression.

4.1.2 Asymmetric vertical loading

In this second load case the internal forces, bending moments and resulting stresses are determined for the situation, whereby half of the surface in longitudinal direction is loaded by the design load (Figure 4.3). For the conventional concrete footbridge designs the resistance to axial forces, shear forces and bending moments are determined and compared to the axial forces, shear forces and bending moments they are exposed to. For the form found concrete footbridge designs the governing stresses, resulting from bending and compression, are compared with the compressive and tensile strength of the concrete. A structure performs efficiently by when the unity check (UC) values are close to, but not higher than 1.0 (i.e. 100% of the material contributes to carrying the load).

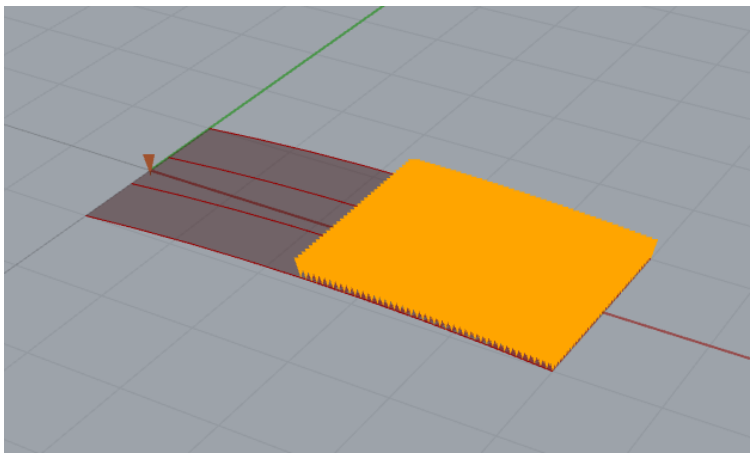

Figure 4.3: Asymmetric vertical load case

Table 4.8 shows the calculation results of the conventional concrete footbridge design for a span of 5 meters. The asymmetric vertical loading case results in a lower maximum shear force and maximum bending moment, compared to the full vertical loading case. Thus, the governing UC-value decreases to 0.73, compared to the 0.89 for the full vertical load. Therefore, design CSB_L5_V3 is sufficient to carry the asymmetric vertical load.

	Properties				Shear force			Bending moment		
	d [mm]	Concrete class	Ø [mm]	s [mm]	V_{Ed} [kN]	V_{Rd} [kN]	UC	M_{Ed} [kNm]	M_{Rd} [kNm]	UC
CSB _L5_ V3	333	C40/50	12	200	40.78	121.91	0.33	46.2	63.21	0.73

**UC = Unity Check – ratio between design force/moment and resisting force/moment*

Table 4.8: Unity check for the conventional concrete footbridge design with a span of 5 m.

Table 4.9 shows the results of the design calculations of the form found concrete footbridge design for a span of 5 meters. Due to the low self-weight of the initial FFB_L5_V design, the asymmetric loading changes the bending moment diagram significantly. As a result, a large tension stress occurs at the bottom of the loaded part of the footbridge, which cannot be carried by the previous design. The new design, FFB_L5_A, has an increased thickness of 70 mm at the supports and 65 mm at the midspans – 55 mm thicker than the original design. The tensile stresses that occur at the bottom of the loaded part of the shell structure, due to bending and axial compression, are governing, with a UC-value of 0.89.

	Properties				Shear force		
FFB_ L5_A	$d_{support}$ [mm]	$d_{midspan}$ [mm]	$h_{midspan}$ [mm]	Concrete class	V_{Ed} [kN]	V_{Rd} [kN]	UC
	70	65	105	C40/50	5.36	65.76	0.08
	Bending + Normal stress (top)			Bending + Normal stress (bottom)			
	$\sigma_{Ed,top}$ [MPa]	f_{cd} [MPa]	UC	$\sigma_{Ed,bottom}$ [MPa]	$f_{ctk,0.05}$ [MPa]	UC	
	7.34	26.67	0.28	2.23	2.5	0.89	

**UC = Unity Check – ratio between design force/moment and resisting force/moment*

Table 4.9: Unity check for the form found concrete footbridge design with a span of 5 m.

The additional utilization check (Figure 4.4) confirms the results given in Table 4.9, with a comparable value of 85.9 %. As can be seen in Figure 4.4, the bottom part of the loaded side and top part of the unloaded side act in tension, and the top part of the loaded side and bottom part of the unloaded side act in compression.

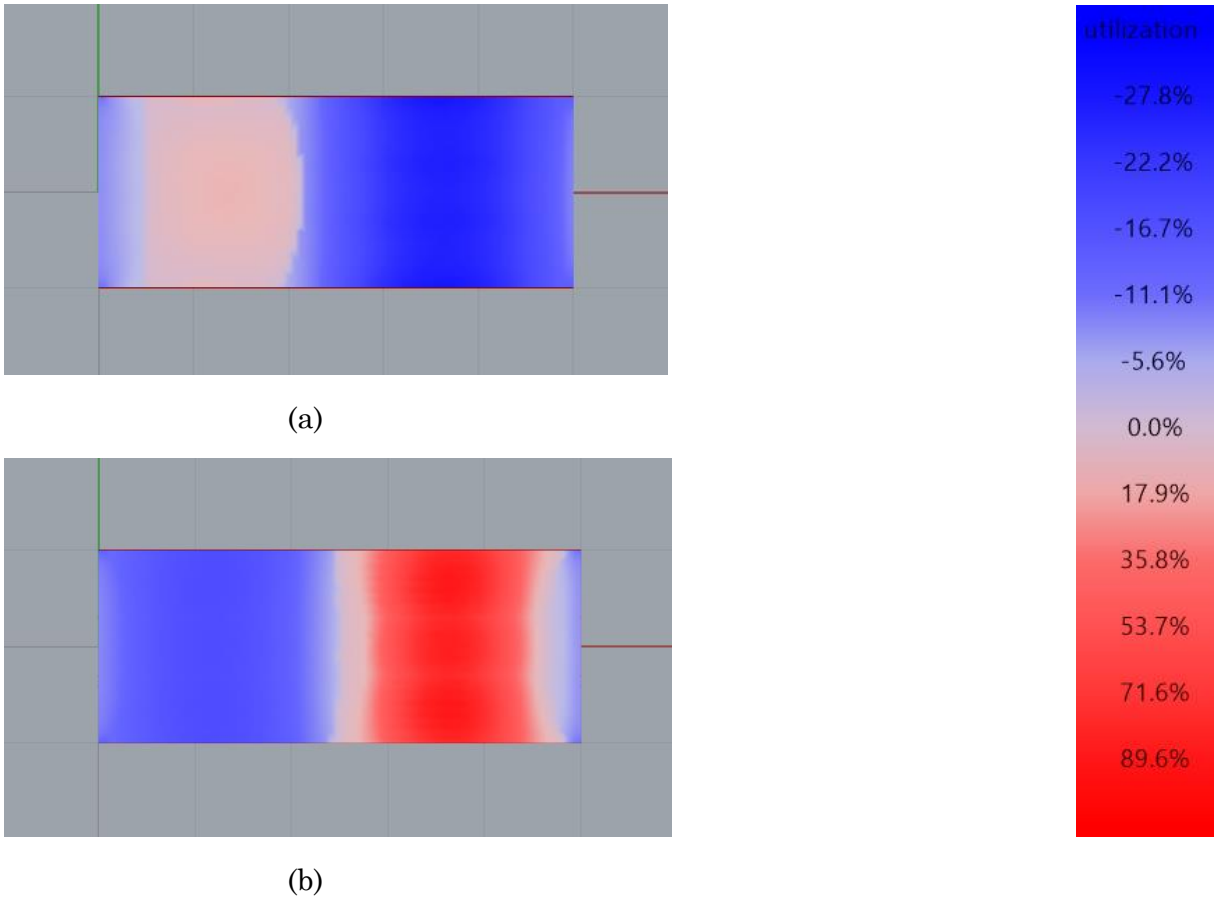

Figure 4.4: Contour plots of the (a) top and (b) bottom of the 5 m long form found concrete footbridge for the asymmetric vertical load, illustrating the utilization rate (blue = compression, red = tension)

Table 4.10 shows the calculation results of the conventional concrete footbridge design for a span of 10 meters. The asymmetric vertical loading case results in a lower maximum shear force and maximum bending moment, compared to the full vertical loading case. Thus, the governing UC-value decreases to 0.85, compared to the 0.96 for the full vertical load. Therefore, design CSB_L10_V2 is sufficient to carry the asymmetric vertical load.

	Properties				Shear force			Bending moment		
	d [mm]	Concrete class	Ø [mm]	s [mm]	V_{Ed} [kN]	V_{Rd} [kN]	UC	M_{Ed} [kNm]	M_{Rd} [kNm]	UC
CSB_L10_V2	667	C50/60	18	167	137.81	264.5	0.52	324.7	381.3	0.85

**UC = Unity Check – ratio between design force/moment and resisting force/moment*

Table 4.10: Unity check for the conventional concrete footbridge design with a span of 10 m.

Table 4.11 shows the results of the design calculations of the form found concrete footbridge design for a span of 10 meters. Due to the low self-weight of the initial FFB_L10_V design, the asymmetric loading changes the bending moment diagram significantly. As a result, a large tension stress occurs at the bottom of the loaded part of the footbridge, which cannot be carried by the previous design. The new design, FFB_L10_A, has an increased thickness of 110 mm at the supports and 105 mm at the midspans – 90 mm thicker than the original design. The tensile stresses that occur at the bottom of the loaded part of the shell structure, due to bending and axial compression, are governing, with an UC-value of 0.99.

	Properties				Shear force		
FFB_ L10_A	$d_{support}$ [mm]	$d_{midspan}$ [mm]	$h_{midspan}$ [mm]	Concrete class	V_{Ed} [kN]	V_{Rd} [kN]	UC
	110	105	210	C50/60	12.61	95.42	0.13
	Bending + Normal stress (top)			Bending + Normal stress (bottom)			
	$\sigma_{Ed,top}$ [MPa]	f_{cd} [MPa]	UC	$\sigma_{Ed,bottom}$ [MPa]	$f_{ctk,0.05}$ [MPa]	UC	
	10.24	33.33	0.31	2.86	2.9	0.99	

**UC = Unity Check – ratio between design force/moment and resisting force/moment*

Table 4.11: Unity check for the form found concrete footbridge design with a span of 10 m.

The additional utilization check confirms the results given in Table 4.11, with a comparable value of 95.7% at the bottom of the loaded part of the footbridge. Similarly, to the contour plot of FFB_L5_A bottom part of the loaded side and top part of the unloaded side act in tension, and the top part of the loaded side and bottom part of the unloaded side act in compression.

Table 4.12 shows the calculation results of the conventional concrete footbridge design for a span of 20 meters. The asymmetric vertical loading case results in a lower maximum shear force and maximum bending moment, compared to the full vertical loading case. Thus, the governing UC-value decreases to 0.92, compared to the 0.98 for the full vertical load. Therefore, design CSB_L20_V2 is sufficient to carry the asymmetric vertical load.

	Properties				Shear force			Bending moment		
	d [mm]	Concrete class	Ø [mm]	s [mm]	V_{Ed} [kN]	V_{Rd} [kN]	UC	M_{Ed} [kNm]	M_{Rd} [kNm]	UC
CSB _L20 _V2	1333	C70/85	25	91	500.6	610.5	0.85	2422	2632	0.92

**UC = Unity Check – ratio between design force/moment and resisting force/moment*

Table 4.12: Unity check for the conventional concrete footbridge design with a span of 20 m.

Table 4.13 shows the results of the design calculations of the form found concrete footbridge design for a span of 20 meters. Due to the low self-weight of the initial FFB_L20_V design, the asymmetric loading changes the bending moment diagram significantly. As a result, a large tension stress occurs at the bottom of the loaded part of the footbridge, which cannot be carried by the previous design. The new design, FFB_L20_A, has an increased thickness of 170 mm at the supports and 165 mm at the midspans – 145 mm thicker than the original design. The tensile stresses that occur at the bottom of the loaded part of the shell structure, due to bending and axial compression, are governing, with an UC-value of 0.97.

	Properties				Shear force		
FFB_ L20_A	$d_{support}$ [mm]	$d_{midspan}$ [mm]	$h_{midspan}$ [mm]	Concrete class	V_{Ed} [kN]	V_{Rd} [kN]	UC
	170	165	415	C70/85	20.82	147.1	0.14
	Bending + Normal stress (top)			Bending + Normal stress (bottom)			
	$\sigma_{Ed,top}$ [MPa]	f_{cd} [MPa]	UC	$\sigma_{Ed,bottom}$ [MPa]	$f_{ctk,0.05}$ [MPa]	UC	
	15.81	46.67	0.34	3.12	3.2	0.97	

**UC = Unity Check – ratio between design force/moment and resisting force/moment*

Table 4.13: Unity check for the form found concrete footbridge design with a span of 20 m.

The additional utilization check confirms the results given in Table 4.13, with a comparable value of 98.0% at the bottom of the loaded part of the footbridge. Similarly, to the contour plot of FFB_L5_A bottom part of the loaded side and top part of the unloaded side act in tension, and the top part of the loaded side and bottom part of the unloaded side act in compression.

As mentioned before, spans longer than 20 meters are not achievable using the conventional concrete footbridge design. Longer spans require alternative construction methods, for example, ZIP-beams.

Table 4.14 shows the results of the design calculations of the form found concrete footbridge design for a span of 45 meters. Due to the low self-weight of the initial FFB_L45_V design, the asymmetric loading changes the bending moment diagram significantly. As a result, a large tension stress occurs at the bottom of the loaded part of the footbridge, which cannot be carried by the previous design. The new design, FFB_L45_A, has an increased thickness of 295 mm at the supports and 290 mm at the midspans – 250 mm thicker than the original design. The tensile stresses that occur at the bottom of the loaded part of the shell structure, due to bending and axial compression, are governing, with an UC-value of 0.93.

	Properties				Shear force		
FFB_ L45_A	$d_{support}$ [mm]	$d_{midspan}$ [mm]	$h_{midspan}$ [mm]	Concrete class	V_{Ed} [kN]	V_{Rd} [kN]	UC
	295	290	940	C90/105	39.34	238.5	0.16
	Bending + Normal stress (top)			Bending + Normal stress (bottom)			
	$\sigma_{Ed,top}$ [MPa]	f_{cd} [MPa]	UC	$\sigma_{Ed,bottom}$ [MPa]	$f_{ctk,0.05}$ [MPa]	UC	
	26.79	60	0.45	3.36	3.5	0.93	

**UC = Unity Check – ratio between design force/moment and resisting force/moment*

Table 4.14: Unity check for the form found concrete footbridge design with a span of 45 m.

The additional utilization check confirms the results given in Table 4.14, with a comparable value of 94.5% at the bottom of the loaded part of the footbridge. Similarly, to the contour plot of FFB_L5_A bottom part of the loaded side and top part of the unloaded side act in tension, and the top part of the loaded side and bottom part of the unloaded side act in compression.

4.1.3 Buckling

For the buckling case, the structure is analysed for the full vertical loading case (Figure 4.1), because this load case results in the maximum axial compression force possible in the structure. Conform an iterative procedure, the thickness of the original footbridge design is increased, until the buckling load factor (BLF) is larger than 1.0 (i.e. no buckling occurs).

The conventional footbridge design transfers the loads to the support by way of bending acting. This causes the structure to not be exposed to axial compression force and therefore unaffected by buckling. On the contrary, the form found footbridge design uses an arch shape to transfer the loads to the support using compressive action. Therefore, buckling is a critical failure mechanism for this design. The BLF is calculated for the first buckling mode (Figure 4.5), as this mode requires the lowest axial compression force to initiate.

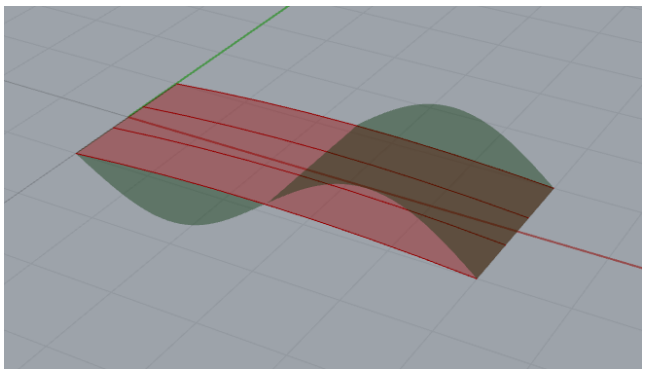

Figure 4.5: First buckling mode of the 5 m long form found concrete footbridge for the full vertical load.

Table 4.15 shows the calculation results for the form found footbridge design with a span of 5 meters. The original design, FFB_L5_V, has a buckling BLF of 0.027, which implies that only 2.7% of the present 251.57 kN is needed to cause the structure to buckling. For the final design, FFB_L5_B, the thickness was increased by 30 mm, which resulted in a BLF of 1.35.

	Properties				Normal force	Buckling Load Factor
	$d_{support}$ [mm]	$d_{midspan}$ [mm]	$h_{midspan}$ [mm]	Concrete class	N_{Ed} [kN]	BLF
FFB_L5_V	15	10	105	C40/50	251.6	0.027
FFB_L5_B	45	40	105	C40/50	357	1.35

Table 4.15: Buckling load factor (BLF) calculation for the form found concrete footbridge designs with a span of 5 m.

Table 4.16 shows the calculation results for the form found footbridge design with a span of 10 meters. The original design, FFB_L10_V, has a BLF of 0.01. For the final design, FFB_L10_B, the thickness was increased by 65 mm, which resulted in a BLF of 1.15.

	Properties				Normal force	Buckling Load Factor
	$d_{support}$ [mm]	$d_{midspan}$ [mm]	$h_{midspan}$ [mm]	Concrete class	N_{Ed} [kN]	BLF
FFB_L10_V	20	15	210	C50/60	520.5	0.01
FFB_L10_B	85	80	210	C50/60	578.9	1.15

Table 4.16: Buckling load factor (BLF) calculation for the form found concrete footbridge designs with a span of 10 m.

Table 4.17 shows the calculation results for the form found footbridge design with a span of 20 meters. The original design, FFB_L20_V, has a BLF of 0.001. For the final design, FFB_L20_B, the thickness was increased by 150 mm, which resulted in a BLF of 1.06.

	Properties				Normal force	Buckling Load Factor
	$d_{support}$ [mm]	$d_{midspan}$ [mm]	$h_{midspan}$ [mm]	Con-crete class	N_{Ed} [kN]	BLF
FFB_L20_V	25	20	415	C70/85	1008.04	0.001
FFB_L20_B	175	170	415	C70/85	1525.01	1.06

Table 4.17: Buckling load factor (BLF) calculation for the form found concrete footbridge designs with a span of 20 m.

Table 4.18 shows the calculation results for the form found footbridge design with a span of 45 meters. The original design, FFB_L45_V, has a BLF of 0.003. For the final design, FFB_L45_B, the thickness was increased by 420 mm, which resulted in a BLF of 1.05.

	Properties				Normal force	Buckling Load Factor
	$d_{support}$ [mm]	$d_{midspan}$ [mm]	$h_{midspan}$ [mm]	Concrete class	N_{Ed} [kN]	BLF
FFB_L45_V	45	40	940	C90/105	2376.49	0.003
FFB_L45_B	465	460	940	C90/105	6079.38	1.05

Table 4.18: Buckling load factor (BLF) calculation for the form found concrete footbridge designs with a span of 45 m.

4.2 Comparison

In this paragraph the final designs of the conventional concrete footbridge and form found concrete footbridge are compared for the different design cases and the different spans. The comparison is based on the amount of material used for each design. An emphasis is put on the amount of concrete used as this is the main material used in both design philosophies.

Table 4.19 shows that if only the full vertical loading is considered, the amount of concrete needed for the form found concrete footbridge is significantly lower – 1.7% to 3.8% of the amount needed for the convention concrete footbridge design. It also shows that when the span increases the amount of concrete needed for the form found concrete footbridge decreases relative to the amount of concrete needed for the conventional concrete footbridge design (i.e. a lower “ratio”).

However, when the asymmetric vertical loading case is also considered Table 4.18 clearly shows an increase in the ratio, going from 1.7% to 3.8% to 20.0% to 12.6%. Once again, as the span increases the “ratio” decreases.

Similarly for the buckling case Table 4.18 shows an increase in the ratio, going from 1.7% to 3.8% to 12.8% to 13.0%. However, for this case an increase of the span cases the “ratio” to increase.

Another observation is that for the spans up to 10 meters, the asymmetric vertical loading is the governing case, however, for spans equal or larger than 20 meters the buckling case becomes governing.

	Span [m]	Concrete [m^3]	Ratio*	Steel [m^3]	Textile [m^2]
CSB_L5_V3	5	3.32		0.006	
FFB_L5_V	5	0.13	3.8%		10 (≈ 5 kg)
FFB_L5_A	5	0.68	20.0%		10 (≈ 5 kg)
FFB_L5_B	5	0.43	12.8%		10 (≈ 5 kg)
CSB_L10_V2	10	13.30		0.031	
FFB_L10_V	10	0.35	2.6%		20 (≈ 10 kg)
FFB_L10_A	10	2.15	16.2%		20 (≈ 10 kg)
FFB_L10_B	10	1.65	12.4%		20 (≈ 10 kg)
CSB_L20_V2	20	53.11		0.22	
FFB_L20_V	20	0.90	1.7%		40 (≈ 20 kg)
FFB_L20_A	20	6.71	12.6%		40 (≈ 20 kg)
FFB_L20_B	20	6.91	13.0%		40 (≈ 20 kg)
FFB_L45_V	45	3.83	-		90.1 (≈ 45 kg)
FFB_L45_A	45	26.35	-		90.1 (≈ 45 kg)
FFB_L45_B	45	41.67	-		90.1 (≈ 45 kg)

** Value expressing the concrete volume used for the form found footbridge design as a percentage of the concrete volume used for the conventional footbridge design.*

Table 4.19. The material-use for the conventional concrete footbridge design and form found concrete footbridge design, for different design cases and spans.

4.3 Discussion

In this paragraph the results presented in the previous paragraphs are interpreted.

In the full vertical load case, the bending moment resistance is governing for all conventional concrete footbridge designs. For the form found designs loaded vertically over the entire span of the bridge, the compressive stresses at the top of the deck are governing. The (small) compressive stress at the top of the deck, resulting from the (small) bending moment, is added to the compressive stress over the entire depth of the deck, stemming from the axial compressive force, to give the resulting governing compressive stress. At

the bottom of the deck the (small) tensile stress, stemming from the (small) bending moment, is added to the compressive stress over the entire depth of the deck, stemming from the axial compressive force, to give a smaller, less governing, resulting compressive stress. For both design types, shear force resistance is not governing due to the presence of a uniformly distributed load (UDL) rather than a point load. In the case of a point load the shear force is concentrated at one location making shear force failures, like punching failure, the governing failure modes.

In the asymmetric vertical load case, the bending moment resistance remains governing for all conventional footbridge designs. However, because the maximum bending moments are smaller than the bending moments in the full vertical load case, the UC results for the conventional concrete footbridge designs loaded asymmetrically are not governing. For the form found designs loaded vertically over the entire span of the bridge, the tensile stresses at the bottom of the loaded part of the deck are governing. The tensile stress at the bottom of the deck, stemming from the know more prominent bending moment, is added to the compressive stress over the entire depth of the deck, stemming from the axial compressive force, to give the resulting governing tensile stress. At the top of the deck the compressive stress, stemming from the bending moment, is added to the compressive stress over the entire depth of the deck, stemming from the axial compressive force, to give a less governing resulting compressive stress. Once again, because the pedestrian bridge is loaded by an UDL, the shear force resistance is not governing for both design types.

All initial form found concrete footbridge designs obtained from the full vertical load case are able to be very slender, because of the high compressive strength of concrete. However, because of this slenderness and the presence of high axial compression force, all designs will fail as a result of instability (i.e. buckling). Therefore, the thickness of the designs has to be increased to increase the buckling resistance. When only considering structural strength, an increase in the strength class of the concrete for each increase of the span was sufficient to require a marginal increase of the footbridge thickness to prevent compressive failure. However, when considering structural stability, as the spans increase so does the slenderness, therefore, requiring significantly thicker decks for longer spans in order to prevent buckling. The result is a minimum increase in thickness of 300% for the 5-meter span and a maximum increase in thickness of 1050% for the 45 meter span.

The amount of concrete used for the shorter span form found footbridge designs of 5 meters and 10 meters, is determined by the governing asymmetric vertical load case. The amount of concrete used for the longer span form found footbridge designs of 20 meters and 45 meters, is determined by the governing buckling load case. This is because the self-weight loads of the short span designs are significantly lower than the variable loads. As a result, the change of the variable load positioning from full to asymmetric, significantly alters the internal stress distribution. As a result, the thickness of the deck needs to be considerably large enough to carry these different stresses. The shorter span designs also naturally are less prone to buckling due to their shorter buckling length. On the other hand, the longer span designs have self-weight closer in magnitude to the variable loads, making the asymmetric vertical load less governing. However, their longer spans cause them to naturally be very slender, making them more susceptible to buckling.

Chapter 5

Conclusions and recommendations

Finite element analyses were conducted in the present thesis to assess the potential reduction of material use by combining shotcrete 3D printing (SC3DP) with the application of textile formworks for the production of form found pedestrian bridges, instead of the conventional design and fabrication process. Using the form found pedestrian bridge design instead of the conventional concrete footbridge design, significantly affects the material use.

The form found footbridge designs with the shorter spans (5 m and 10 m) are determined by the tensile stresses at the bottom of the deck in asymmetric vertical load case, whereas the designs with the longer spans (20 m and 45 m) are determined by the buckling case. The conventional concrete footbridge designs are limited to spans up to 20 meters, whereas the form found designs can reach the prefabrication limit of 45 meters. The final form found concrete pedestrian bridge designs only require a fraction of the concrete used for the conventional concrete pedestrian bridge designs: 20.0%, 16.2% and 13.0% for spans of 5 m, 10 m and 20 m, respectively.

It should be noted that the design calculations were only limited to three cases. In order to obtain realistic designs, the dynamic effects of pedestrians should be considered as well. However, the general approach for determining user induced vibrations at the design stage requires the designer to build a numerical model. This is separate process that did not fit in the scope of this thesis.

Future research can look into these dynamic effects and determine how they influence the design. Other more detailed load aspects that can be studied are, for example, railings, accidental (point) loads and transportation (point) loads. In terms of design, future studies can also assess how the form found concrete footbridge design performs compared to other innovative concrete footbridge designs.

Bibliography

Adapa (2022), 'Adaptive moulds', online [accessed 13.06.2022]. URL: https://adapa.dk

Adriaenssens, Sigrid, Block, Philippe, Veenendaal, Diederik, Williams, & Chris. (2014). *Shell Structures for Architecture: Form Finding and Optimization*.

American Association of State Highway and Transportation Officials. (2009). *LRFD guide specifications for the design of pedestrian bridges*.

Amir, O., & Shakour, E. (2018). Simultaneous shape and topology optimization of prestressed concrete beams. *Structural and Multidisciplinary Optimization*, *57*(5), 1831–1843. https://doi.org/10.1007/s00158-017-1855-5

Balz, M. (2022), online [accessed 15.06.2022]. URL: http://www.michael-balz.de

British Standards Institution. (2018). *Design of an accessible and inclusive built environment. Part 2 Buildings. Code of practice*.

Caron, J. F., Julich, S., & Baverel, O. (2009). Selfstressed bowstring footbridge in FRP. *Composite Structures*, *89*(3), 489–496. https://doi.org/10.1016/j.compstruct.2008.11.009

Castaldelli, V. N., Tashima, M. M., Melges, J. L., Akasaki, J. L., Monzó, J., Borrachero, M. v., Soriano, L., & Payá, J. (2014). *Preliminary studies on the use of sugar cane bagasse ash (SCBA) in the manufacture of alkali activated binders*.

Clark, J. H., Abdou, H. M., Allen, J. H., Anderson, G. H., Arbabi, F., Ballinger, C. A., Barker, J. M., Bender, O., Campbell, T. I., Cannon, J., Carnegie, C. A., Carrato, J. L., Chadha, G., Corley, W. G., Davidge, W. M., Drugge, H. E., Epp, W. H., Everard, N. J., & Felder, A. L. (1995). *Analysis and Design of Reinforced Concrete Bridge Structures Reported by ACI-ASCE Committee 343*.

Dennis, R. (2015). *Footbridges A Manual for Construction at Community and District Level*. https://www.researchgate.net/publication/242538513

Descamps, B., Filomeno Coelho, R., Ney, L., & Bouillard, P. (2011). Multicriteria optimization of lightweight bridge structures with a constrained force density method. In *Computers and Structures* (Vol. 89, Issues 3–4, pp. 277–284). https://doi.org/10.1016/j.compstruc.2010.11.010

Eurocode 2. (2004). *Eurocode 2: Design of concrete structures - Part 1-1: General rules and rules for buildings*.

Fauche, E., Adriaenssens, S., & Prevost, J. H. (2010). Structural optimization of a thin-shell bridge structure. In *Article in Journal of the International Association for Shell and Spatial Structures*. https://www.researchgate.net/publication/264886208

Fenu, L., Congiu, E., Marano, G. C., & Briseghella, B. (2020). Shell-supported footbridges. *Curved and Layered Structures*, *7*(1), 199–214. https://doi.org/10.1515/cls-2020-0017

García de Soto, B., Agustí-Juan, I., Hunhevicz, J., Joss, S., Graser, K., Habert, G., & Adey, B. T. (2018). Productivity of digital fabrication in construction: Cost and time analysis of a robotically built wall. *Automation in Construction*, *92*, 297–311. https://doi.org/10.1016/J.AUTCON.2018.04.004

Grünewald, S., Schipper, R., & Hordijk, D. (2015). *Double-curved panels produced in a flexible mould with self-compacting fibre-reinforced concrete*.

Hack, N., & Kloft, H. (2020). Shotcrete 3D Printing Technology for the Fabrication of Slender Fully Reinforced Freeform Concrete Elements with High Surface Quality: A Real-Scale Demonstrator. In *RILEM Bookseries* (Vol. 28, pp. 1128–1137). Springer. https://doi.org/10.1007/978-3-030-49916-7_107

Halpern, A. B., & Adriaenssens, S. (2015). In-plane optimization of truss arch footbridges using stability and serviceability objective functions. *Structural and Multidisciplinary Optimization*, *51*(4), 971–985. https://doi.org/10.1007/s00158-014-1187-7

Hoppermann, M., Reuvers, H., Nap, P., & van Overveld, B. (2015). *Design to Installation of a free-form roof cladding with a flexible mould. The building of the public transport terminal Arnhem*.

Kloft, H., Krauss, H. W., Hack, N., Herrmann, E., Neudecker, S., Varady, P. A., & Lowke, D. (2020). Influence of process parameters on the interlayer bond strength of concrete elements additive manufactured by Shotcrete 3D Printing (SC3DP). *Cement and Concrete Research*, *134*. https://doi.org/10.1016/j.cemconres.2020.106078

Kristensen, M. K., & Raun, C. (2011). *A flexible mat for providing a dynamically reconfigurated double-curved moulding surface in a mould* (Patent No. US 9,168,678 B2).

Kromoser, B., & Kollegger, J. (2014). Building shell structures out of reinforced concrete using the "Pneumatic Wedge Method" | Herstellung von Schalentragwerken aus Beton mit der "pneumatic Wedge Method." *Beton- Und Stahlbetonbau*, *109*(8), 557–565. https://doi.org/10.1002/best.201400014

Meyer, C. (2004). Concrete materials and Sustainable Development in the USA. *Structural Engineering International: Journal of the International Association for Bridge and Structural Engineering (IABSE)*, *14*(3), 203–207. https://doi.org/10.2749/101686604777963757

Neff, W. (1941). *Building Construction* (Patent No. US 2,270229).

Parke, G. A. R., Hewson, N. R., & Institution of Civil Engineers (Great Britain). (2008). *ICE manual of bridge engineering*.

Pipinato, A. (2022). Footbridges. *Innovative Bridge Design Handbook: Construction, Rehabilitation and Maintenance*, 621–634. https://doi.org/10.1016/B978-0-12-823550-8.00013-5

Popescu, M. A. (2019). *KnitCrete Stay-in-place knitted formworks for complex concrete structures*. ETH Zürich.

Quagliaroli, M., & Malerba, P. G. (2013). Flexible bridge decks suspended by cable nets. A constrained form finding approach. *International Journal of Solids and Structures*, *50*(14–15), 2340–2352. https://doi.org/10.1016/j.ijsolstr.2013.03.009

Raun, C., & Kirkegaard, P. H. (2015). *Adaptive Mould-A Cost-Effective Mould System Linking Design and Manufacturing of Double-Curved GFRC Panels*. www.adapa.dk

Rhode-Barbarigos, L., Hadj Ali, N. B., Motro, R., & Smith, I. F. C. (2010). Designing tensegrity modules for pedestrian bridges. *Engineering Structures*, *32*(4), 1158–1167. https://doi.org/10.1016/j.engstruct.2009.12.042

Salet, T. A. M., Ahmed, Z. Y., Bos, F. P., & Laagland, H. L. M. (2018). Design of a 3D printed concrete bridge by testing*. *Virtual and Physical Prototyping*, *13*(3), 222–236. https://doi.org/10.1080/17452759.2018.1476064

Schipper, H. R., Grünewald, S., Eigenraam, P., Raghunath, P., & Kok, M. A. D. (2015). *Production of Curved Precast Concrete Elements for Shell Structures and Free-form Architecture using the Flexible Mould Method*.

Segal, E. M., Rhode-Barbarigos, L., Adriaenssens, S., & Filomeno Coelho, R. D. (2015). Multi-objective optimization of polyester-rope and steel-rope suspended footbridges. *Engineering Structures*, *99*, 559–567. https://doi.org/10.1016/j.engstruct.2015.05.024

Vantyghem, G., de Corte, W., Shakour, E., & Amir, O. (2020). 3D printing of a post-tensioned concrete girder designed by topology optimization. *Automation in Construction*, *112*. https://doi.org/10.1016/j.autcon.2020.103084

Veenendaal, D., & Block, P. (2012). An overview and comparison of structural form finding methods for general networks. *International Journal of Solids and Structures*, *49*(26), 3741–3753. https://doi.org/10.1016/J.IJSOLSTR.2012.08.008

Vollers, K., & RIetbergen, D. (2009). *A method and apparatus for forming a double-curved panel form a flat panel* (Patent No. WO 2009/002158 A1).

Wolfs, R. J. M., Bos, F. P., & Salet, T. A. M. (2019). Hardened properties of 3D printed concrete: The influence of process parameters on interlayer adhesion. *Cement and Concrete Research*, *119*, 132–140. https://doi.org/10.1016/j.cemconres.2019.02.017